WADD-TR-60-475
Part II

COLLISIONS OF LIQUID DROPS WITH LIQUIDS

PART II.—CRATER DEPTH IN FLUID IMPACTS

TECHNICAL REPORT NO. WADD-TR-60-475, Part II

NOVEMBER 1962

DIRECTORATE OF MATERIALS AND PROCESSES
AERONAUTICAL SYSTEMS DIVISION
AIR FORCE SYSTEMS COMMAND
WRIGHT-PATTERSON AIR FORCE BASE, OHIO

Project No. 7342, Task No. 734202

(Prepared under Contract No. AF 33(657)-62-385
by the National Bureau of Standards Washington, D. C.;
Olive G. Engel, author)

NOTICES

When Government drawings, specifications, or other data are used for any purpose other than in connection with a definitely related Government procurement operation, the United States Government thereby incurs no responsibility nor any obligation whatsoever; and the fact that the Government may have formulated, furnished, or in any way supplied the said drawings, specifications, or other data, is not to be regarded by implication or otherwise as in any manner licensing the holder or any other person or corporation, or conveying any rights or permission to manufacture, use, or sell any patented invention that may in any way be related thereto.

ASTIA release to OTS not authorized.

Qualified requesters may obtain copies of this report from the Armed Services Technical Information Agency, (ASTIA), Arlington Hall Station, Arlington 12, Virginia.

Copies of this report should not be returned to the Aeronautical Systems Division unless return is required by security considerations, contractual obligations, or notice on a specific document.

FOREWORD

This report was prepared by the National Bureau of Standards, Washington, D. C., on Air Force Contract AF 33(657)-62-385, under Task No. 734202, "Studies on the Structure-Property Relationships of Polymeric Materials", of Project No. 7342, "Fundamental Research on Macromolecular Materials and Lubrication Phenomena." The contract efforts were accomplished under the cognizance of the Directorate of Materials and Processes, Aeronautical Systems Division, with the technical work directed by Lt. Charles Katsikas as project engineer.

ABSTRACT

Results of the use of high-speed and low-speed motion picture photography and of high-speed color photography to determine the flow configuration of both the drop and target liquids, when a liquid drop impinges against a body of liquid, are described. A theoretical treatment of the depth of the cavity that forms in a target liquid as a result of the impact of a liquid drop is developed. Results of preliminary tests of the equation are presented and discussed.

PUBLICATION REVIEW

This report has been reviewed and is approved.

FOR THE COMMANDER:

H. S. Schwartz

H. S. SCHWARTZ
Chief, Plastics and Composites Branch
Nonmetallic Materials Laboratory
Directorate of Materials and Processes

TABLE OF CONTENTS

LIST OF ILLUSTRATIONS

LIST OF TABLES

1. Introduction

Velocity is the parameter that determines the room-temperature behavior of matter during impact. If a ductile metal sphere is fired against a solid target at increasingly higher velocities, a velocity is finally reached at which permanent deformation results. If the impingement velocity is increased further, such a sphere will flow radially during the impact as though it were liquid and the event is a special case of impact of a liquid drop against a solid. If the impact velocity is increased still further, liquefaction not only of the impinging sphere but also of the solid target occurs and the event is an imperfectly developed case of impact of a liquid drop against a liquid [1]. [a]

Meteorites travel at enormous velocities and it has been postulated [2] that when they collide with a solid object liquefaction both of the meteorite and of the solid object at the immediate site of the collision occurs. The event has been characterized [2] as impact of a liquid drop of density δ into a liquid medium of density ρ. Because erosion craters may be produced on space vehicles as a result of collision with micrometeorites, and because these collisions may be liquid-type collisions at least in their initial stages, it is of current interest to be able to predict the depth of the craters that form in collisions of this kind.

It has been postulated [3] that a study of free-fall-velocity impact of liquid drops against a body of liquid may produce information of value for the high-velocity liquefied-drop and liquefied-target case. Although 80 years have passed since Worthington [4,5,6] carried out his classic investigation of impact of liquid drops against liquids, even the simplest example of this type of impact (waterdrops falling into water) is very poorly understood.

---

[a] Numbers in brackets refer to literature references at the end of this paper.

Manuscript released by the author October 1962 for publication as a WADD Technical Report.

Work that is described in the following sections have been done to throw further light on this type of impact.

2. Flow of the Drop Liquid

In order to determine what happens to the original liquid of a drop that impinges against a body of liquid, five high-speed color moving pictures were taken[b] of the impact of a drop of red ink against colorless water.

For two of these color moving pictures the target water was placed in a rectangular vessel having glass sides. It was approximately 7 in. wide, 12 in. long, and 9 in. high and was filled to a depth of about 6 in. with distilled water. The drops of red ink were allowed to fall approximately 9 ft through air at atmospheric pressure before they impinged against the water surface. The impact phenomena were photographed with use of a microsecond stroboscope synchronized with a moving strip of film.

For three of the color moving pictures distilled water was admitted into the target-liquid tank of the NBS liquid-drop accelerator apparatus[c] to a depth of approximately 12 in. The total pressure above the water surface was 37 to 38 mm of mercury during the course of the impacts. The temperature was 19.8° C. The drops of red ink fell a distance of 63.5 ft through the liquid-drop accelerator apparatus under these conditions of temperature and pressure before they impinged against the water surface.

---

[b] These pictures were taken under the direction of Mr. T. C. Hellmers and Mr. Ralph Berry of Diamond Ordnance Fuse Laboratory.

[c] A preliminary description of this apparatus is given in Reference [3]. It is described in more detail in section 6 of this paper.

Two cameras were used to photograph the impacts for the second experimental arrangement. One was placed to view the impacts from the side, and as for the first two color moving pictures, the impacts were photographed with use of a microsecond stroboscope that was synchronized with the moving film strip in the camera. The second camera, which was triggered simultaneously with the first, was located below the target liquid tank. It viewed the impacts directly from below.

Study of the films that were made in both experimental arrangements produced the following information.

The first cavity that forms in the target liquid after the impact has occurred is a very shallow sheer-walled cylinder with flat bottom. In the first frame in which a cavity can be seen in the moving pictures taken from the side, the red liquid of the drop appears to have spread over the bottom of this cavity; the upper surface of the flow of the drop liquid is obscured by the meniscus of the target liquid. The shallow disk-like cavity rapidly becomes hemispherical in shape and the red liquid of the drop spreads over the lower surface of the hemisphere as can be seen from the four successive frames of one of the moving pictures (taken from below the impact) that are shown in Figure 1.

In these pictures the irregular light-colored central mass is the red liquid of the drop. The light-colored circle around the spreading drop is an artifact. It is present before the red drop appears and consequently is not the periphery of the cavity in the target liquid. It is noteworthy that the bottom surface of the radially flowing drop, as seen in these pictures, is not always a featureless enlarging circle. In picture B there is evidence of

A

B

C

D

Figure 1. Radial flow of a drop of red ink after impact against water as viewed from below

radial striations in what appears to be an almost planar disk, but in pictures C and D lobes or points appear to have developed. The appearance of lobes may be an artifact produced by the flow of the target water under the impinging drop. However, the observation is of interest because in later stages of the development of the cavity, as viewed from the side, prongs of red drop liquid appear, as will be discussed later. Furthermore, in craters produced by hypervelocity impact of copper spheres against aluminum targets, prongs of copper appear to have been forced into the aluminum target at the bottom and along the lower sides of the crater.

Very little useful information can be obtained from the frames of the moving picture subsequent to picture 4 of Figure 1. This seems to be the result of interference provided by the flow of the target liquid as it recedes from the central point of the impact and the cavity increases in size. The flow of the target liquid is discussed in section 3 below.

The flow of the red drop within the enlarging cavity produced in the target liquid by the impact cannot be seen in the moving pictures taken by the camera that viewed the impacts from the side. The phenomena were lighted from behind and the enlarging cavity appears black in the pictures. However, the location of the drop liquid can be deduced from observations discussed below.

The crown of liquid that rises at the periphery of the cavity formed in the target liquid is obscured by the meniscus of the target liquid in the first frame in which a cavity is visible but it can be seen in the following frame. It is essentially colorless. The standing crown of liquid is, therefore, formed out of target liquid and not out of drop liquid although a slight pink tinge, especially in the lower velocity impacts, suggests that a boundary layer of drop liquid may be carried into it. The fact that the liquid crown at the periphery of the cavity consists of target liquid and not

of drop liquid leads to the conclusion that this liquid crown is a cylindrical wave in the target liquid. It will be referred to hereafter as the cylindrical wave. The source of the target liquid that feeds this wave is discussed in section 3 below.

In later frames of the moving pictures of the low-velocity impacts, streaks of red drop liquid can be seen in the cylindrical wave and streamers of red drop liquid are visible in the high light located in the upper third of the cavity. Red streamers can also be seen moving out of the hemispherical wall of the cavity into the colorless target liquid. Because of the difficulty in reproducing color photographs, the location of the red streamers will be shown by comparison of picture A and picture B of Figure 2.

Figure 2B shows a stage of the splash configuration of a drop of red ink that impinged at low velocity against colorless water. Figure 2A shows a similar stage for the impact of a colorless waterdrop against water. The protruding bumps on the hemispherical surface of the cavity in Figure 2B, which are absent in Figure 2A, appear red when white light is passed through the color film. They are streamers of red drop liquid that have moved out into the colorless target liquid. The existence of these protrusions of drop liquid was referred to in discussing the lobes that appear to exist on the under surface of the drop after impact as seen in picture B of Figure 1.

There are several plausible explanations for the existence of these prongs of drop liquid. The most appealing of these, from the standpoint of impact mechanics, is that the curved trailing surface of the drop focuses the tension wave that reflects from it. A pressure pulse is initiated in the drop by the impact; it moves through the drop and is reflected from the free trailing surface of the drop as a tension wave. This tension wave moves back to the impact surface. Because the curved trailing surface of the drop is changing in shape with elapsed time, the returned tension waves are focused over

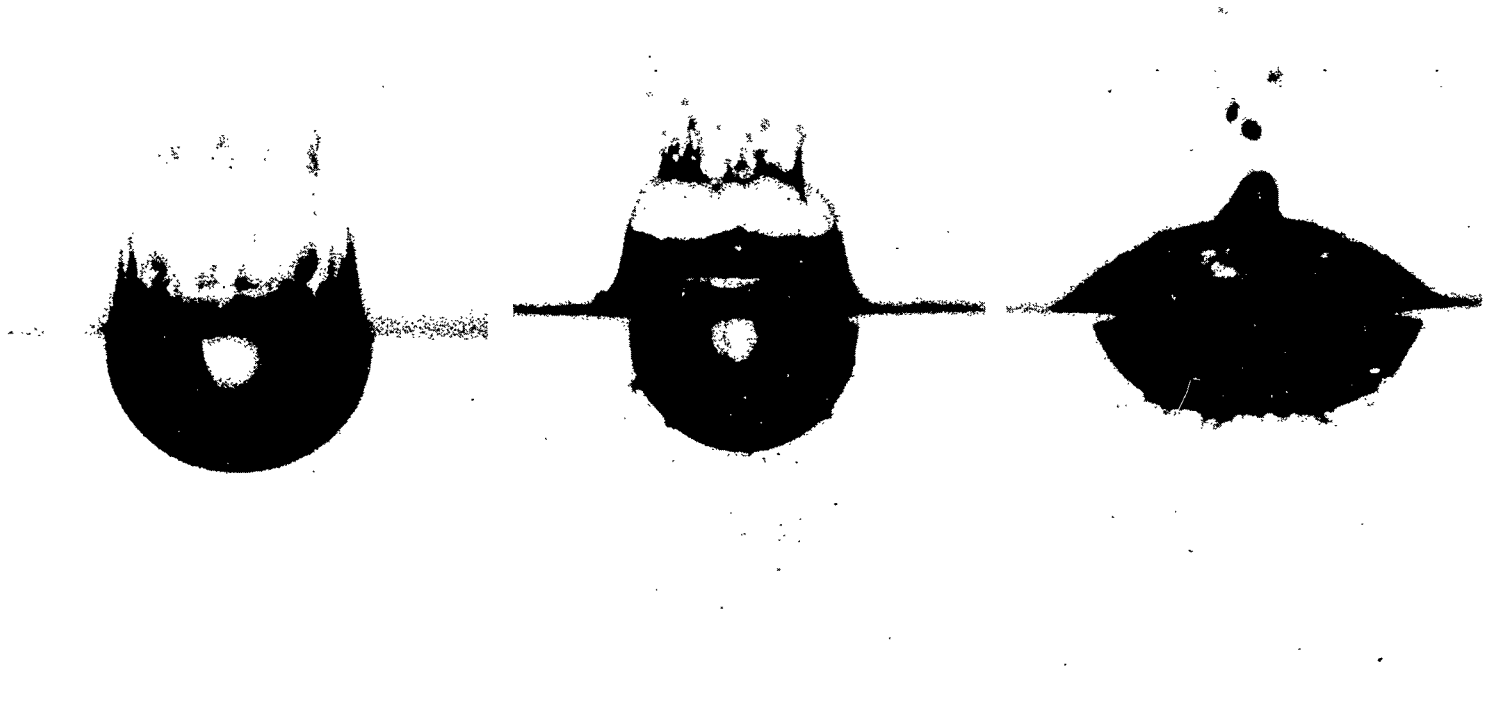

Figure 2. Spash caused by a waterdrop and by a drop of red ink as a result of impact with water

A. Impact of waterdrop with water; cavity is approaching maximum size
B. Impact of drop of red ink with water; cavity is approaching maximum size
C. Impact of drop of red ink with water; a later stage in which a bubble has formed over the cavity

an area. The maximum pressure that is developed by the impact exists in a circle around the central point of impact and it is reasonable to suppose that the maximum in the returned tension wave will also exist in a circle of maximum tension within the area over which they are focused. This reasoning would account for a ring of maximum tension. However, it is not clear why there should be lobes, or points of maximum tension on the ring of maximum tension. It is conceivable that this may be the result of some kind of symmetrical interference in the superposition of the reflected waves.

Another possible explanation is that the isolated protuberances of drop liquid may indicate the presence of eddies at points on the hemispherical surface of the cavity in the target liquid; this cavity is increasing rapidly in size and the flow about it, as the target liquid recedes from the central point of impact, may be turbulent.

Finally, it is possible that the points at which protuberances of drop liquid originate may correspond to the leading tips of rapidly moving streams in the radial flow of the drop. Such rapidly moving streams are known to be present in the radial flow of a drop that impinges against the planar surface of a solid [7].

The structures in the cavity high-light in Figure 2B, which are absent in Figure 2A, are streamers of red drop liquid that are flowing up the hemispherical wall of the cavity. Streamers of red drop liquid can also be seen in the cylindrical wave in Figure 2B. Similar streaks can be seen in the cylindrical wave in Figure 2A due to streamers from the radial flow of the colorless waterdrop but these are less well defined than the red streamers seen in Figure 2B.

The above observations indicate that the bulk of the drop liquid remains in the lower half of the cavity. Only streamers from the radial flow of the drop liquid are visible in the cavity high light in the upper

third of the cavity wall and in the cylindrical wave. If the red drop liquid had spread over the entire cavity in the target liquid, the cavity high light would have been obliterated. The red streamers that have been pointed out are less apparent in the moving picture of the impact of a drop of red ink against water when the fall height was 63.5 ft than when the fall height was approximately 9 ft. The cylindrical wave is much higher and of greater diameter for the higher impact velocity.

Shortly after the cavity reaches maximum size, the top of the cylindrical wave constricts under the action of surface tension to form a bubble over the cavity. In the moving picture of the low-velocity impact, the water masses at the top of the closed bubble are spotted with red drop liquid which indicates that the streamers of drop liquid reached the top of the cylindrical wave. Figure 2C shows an advanced stage of this configuration for the low-velocity impact of a drop of red ink with water. The small protuberances of the hemispherical wall of the cavity in Figure 2B consist of red drop liquid that is beginning to diffuse into the colorless target liquid; they have grown into long whisker-like structures at the bottom of the shallowing cavity in Figure 2C. The fact that these structures are restricted to the lower half of the cavity in Figure 2C confirms the conclusion that the bulk of the drop liquid remains in the lower half of the cavity.

After the cylindrical wave has constricted to form a bubble over the cavity, the water masses at the point of closure coalesce into a jet that begins to move downward toward the surface of the target liquid. An upward-moving jet also begins to rise from the center of the cavity floor. These jets eventually meet and merge. The mechanism by which the upward-moving jet is formed is discussed in section 3. Figure 3A shows the upward-moving jet rising from the center of the cavity floor. Figure 3B shows the

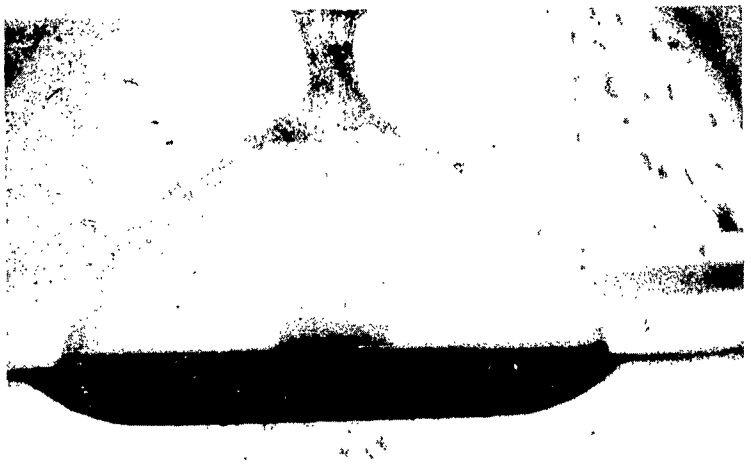

A

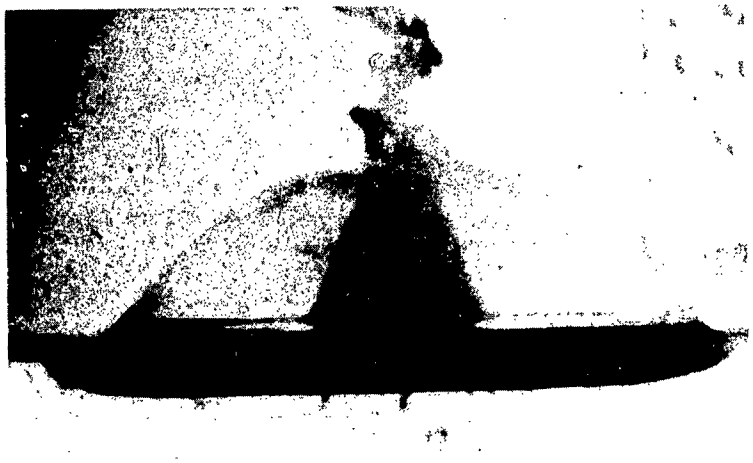

B

Figure 3. Late stages in the impact of a drop of red ink with water

A. Colorless jet rises from center of cavity floor
B. The upward-moving jet merges with a jet that moves downward from the apex of the bubble

splash configuration of high-velocity liquid drop impacts (a bubble containing a central column of liquid) after the jets have met and merged. Figures 3A and 3B are enlargements of frames from a color moving picture of the high-velocity impact of a drop of red ink with colorless water. In projections of the color film the upward-moving jet in the center of the cavity floor in Figure 3A is light gray in color but the protruding whisker-like structures of diffused drop liquid at the bottom of the cavity are red. One of the red tentacles appears to have coiled into a circle, which adds some strength to the suggestion that these structures may form as a result of eddies.

Worthington [6] has reported that when a drop of milk falls a distance of 100 cm into water, the upward-moving jet that forms carries at its apex the white liquid of the milk drop that impinged. On the basis of this information it would be expected that the apex of the upward-moving jet in Figure 3A should be red. Unfortunately the red ink that was used for the drop was so concentrated that, in the frames in which the drop itself can be seen before it strikes the water surface, the freely falling drop has no high light and it furthermore appears to be light gray when white light is passed through the film just as the rising jet in the views of Figure 3 appears to be light gray. Consequently, it is possible that the concentration of ink at the apex of the jet is sufficient to make it essentially an opaque object and to mask its color. The point as to whether or not the red liquid of the drop is at the apex of this jet for high-velocity collisions (approximately 55 ft/sec) of liquid drops with liquids, as has been reported for low-velocity collisions, should be clarified, and it is hoped that it will be possible to do this with a less intense red drop at a later time.

3. Flow of the Target Liquid

The flow that takes place in a body of liquid when a liquid drop impinges against it was studied by means of low-speed motion pictures of

waterdrops impinging against a suspension of white particles. Any motion of the liquid that supported the particles was registered as streaks in the separate frames of the moving pictures because of the motion of the particles themselves.

The suspension, which consisted of particles of a white plastic in a water-alcohol solution, was placed in a small glass cell that had parallel sides. See Figure 4. Use of a small cell reduced loss of definition due to light scattering by the plastic particles. To inhibit settling of the suspended particles, the concentration of the water-alcohol solution was adjusted so that its density was equal to that of the particles. Because the plastic particles had a range of densities, a certain amount of settling was unavoidable.

Motion pictures of waterdrops impinging against the suspension were taken[d] at rates of 64, 32, and 8 frames per second. The impact phenomena were lighted from the front and side. Figure 5 shows a very early stage of the impact taken at a frame rate of 64 per second. In this picture the cavity depth is only slightly less than its radius and the cavity is approaching a hemisphere in shape. There is hardly any motion indicated in the target liquid.

Figure 6 shows a slightly later stage of the initial growth of the cavity and cylindrical wave taken at the same frame rate. Streamlines that move radially outward and upward from points on the lower half of the cavity are just barely discernible in this picture.

These streamlines are well defined in the later stage of cavity growth shown in Figure 7A which was photographed at the same frame rate. They are even more clearly defined in Figure 7B for which the frame rate was only half

[d]These pictures were taken by Mr. Manuel Costa of NBS photolaboratory.

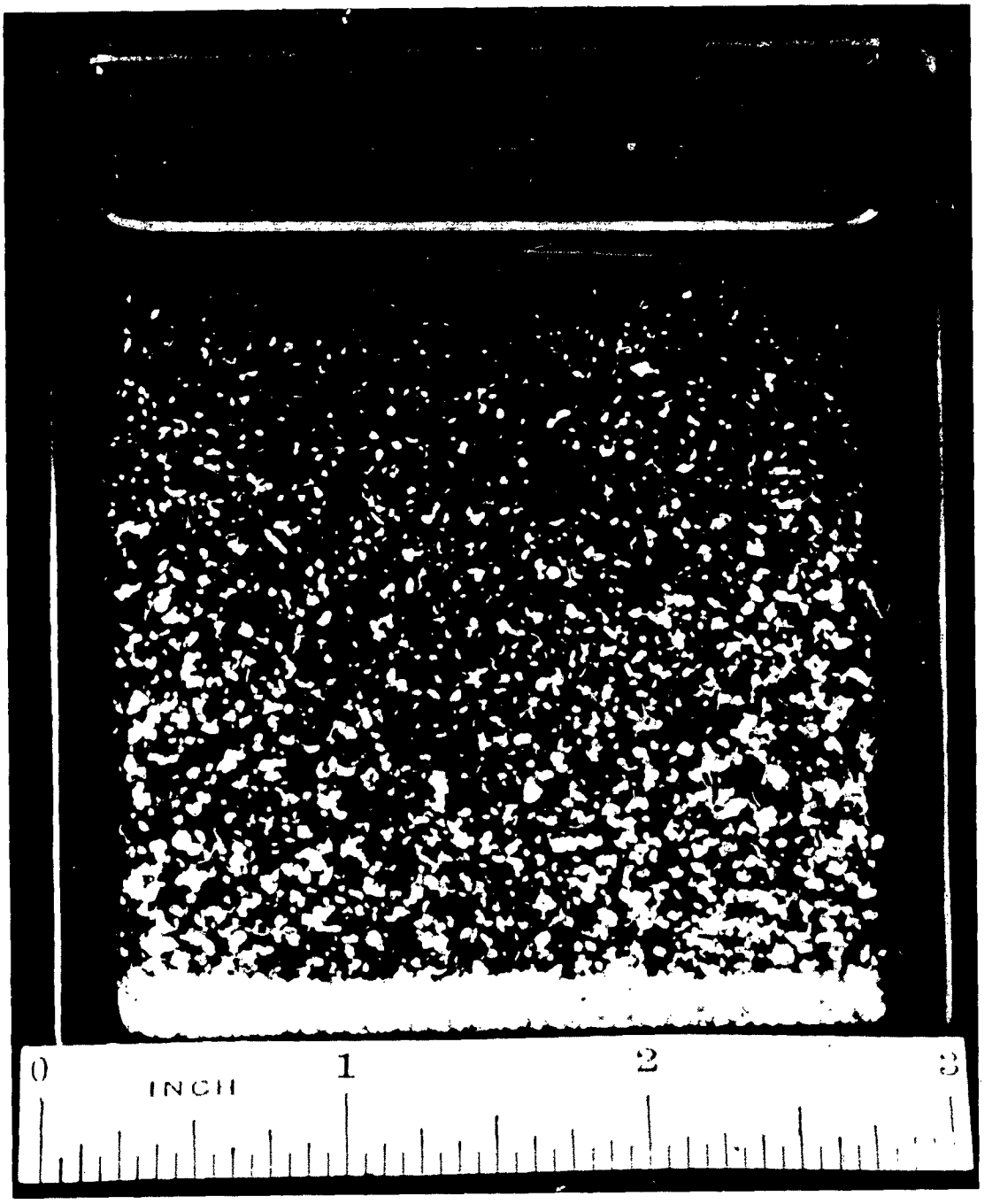

Figure 4. Rectangular cell containing suspension of plastic particles

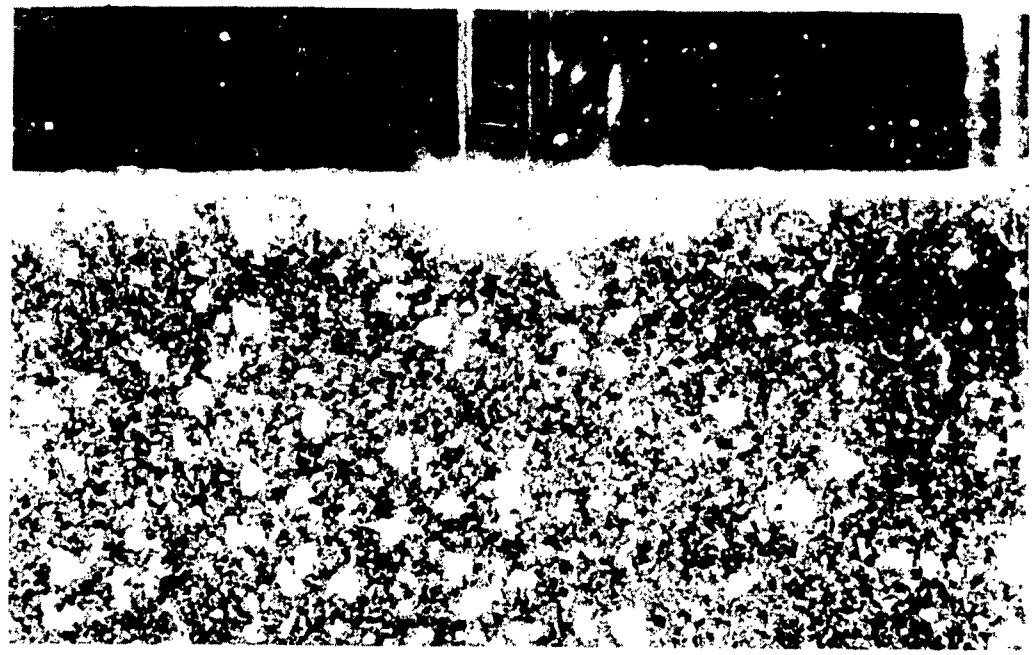

Figure 5. First stage of the impact (64 frames/sec)

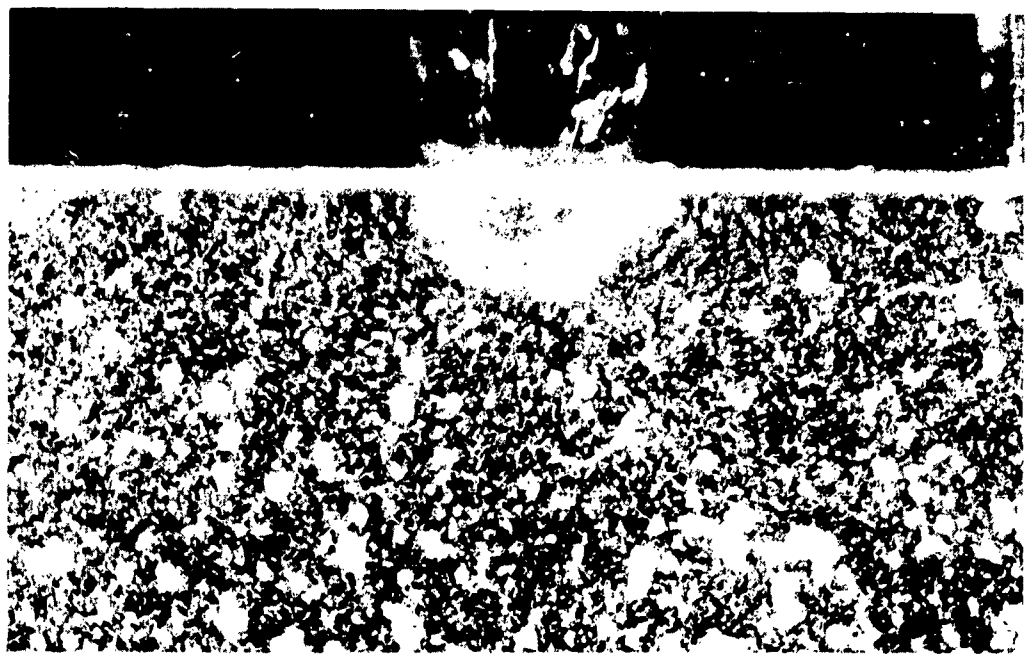

Figure 6. Initial growth of cavity and cylindrical wave (64 frames/sec)

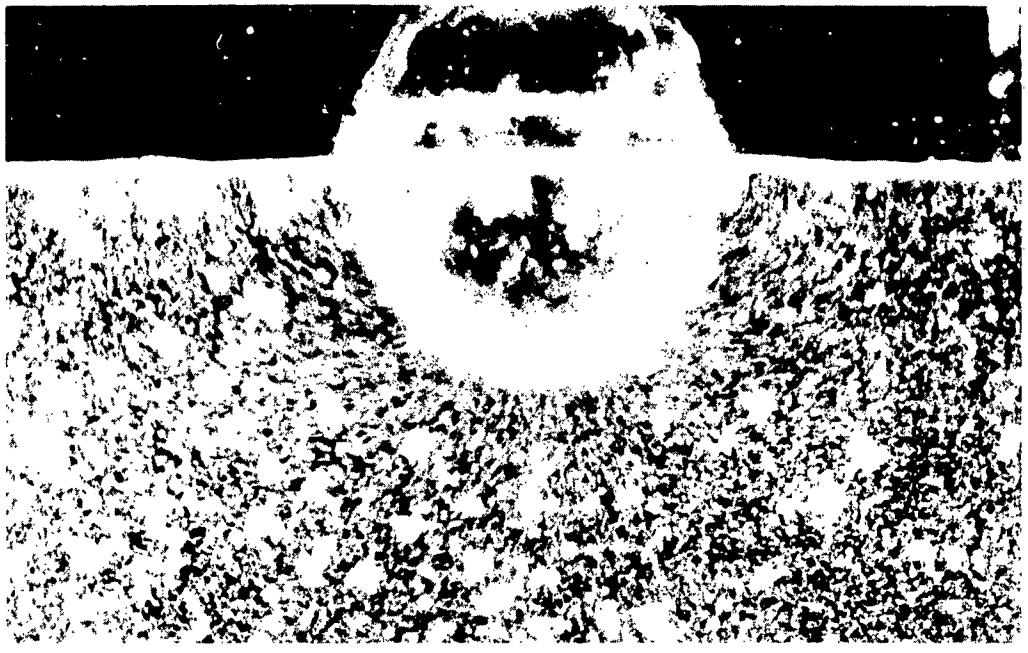

View A (64 frames/sec)

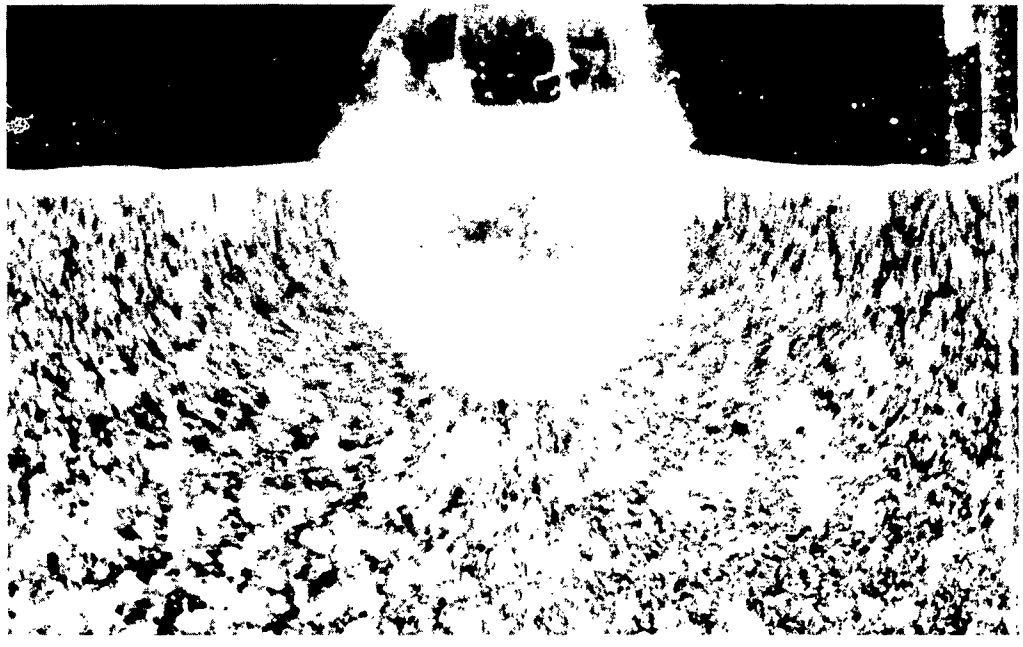

View B (32 frames/sec)

Figure 7. Enlarging cavity approaches maximum size

as great. In Figures 7A and 7B the enlarging cavity is approaching maximum size. The crest of the cylindrical wave at the periphery of the cavity is unfortunately beyond the top of the frame. It may already have constricted under the action of surface tension and closed to form a bubble.

Figures 8 and 9 show the cavity slightly after it has reached maximum size. Motion in the target liquid is at a standstill. The downward-moving jet, which appears after the crest of the cylindrical wave has closed to form a bubble, is just forming in Figure 8. Figure 9 shows the downward-moving jet in a well-developed state; it has progressed nearly half-way through the cavity in the target liquid.

Figure 10 shows the streamlines in the recovery motion of the target liquid. The direction of motion is now downward and inward toward the lower half of the cavity floor. The dynamic recoil of the target liquid, shown in Figure 10, affords an explanation for the upward-moving liquid jet in the center-bottom of the cavity floor that has been observed in high-speed pictures of liquid drops impinging against liquids. See Figure 3A. The upward- and downward-moving jets eventually collide and merge. This stage may have been reached in Figure 11, which was taken at slow speed, but details in the lower half of the cavity in this figure are obscured.

The well-defined streamlines in Figure 11, taken at the lowest frame rate that was used in this study, show that marked motion in the target liquid occurs radially around the cavity to the extent of about one cavity radius beyond the cavity wall.

The evidence obtained from this study of impacts of waterdrops against a suspension of white particles indicates that the flow produced in a liquid as a result of the impact of a liquid drop does not have the spherical symmetry of the flow of an infinite mass of liquid around an expanding bubble

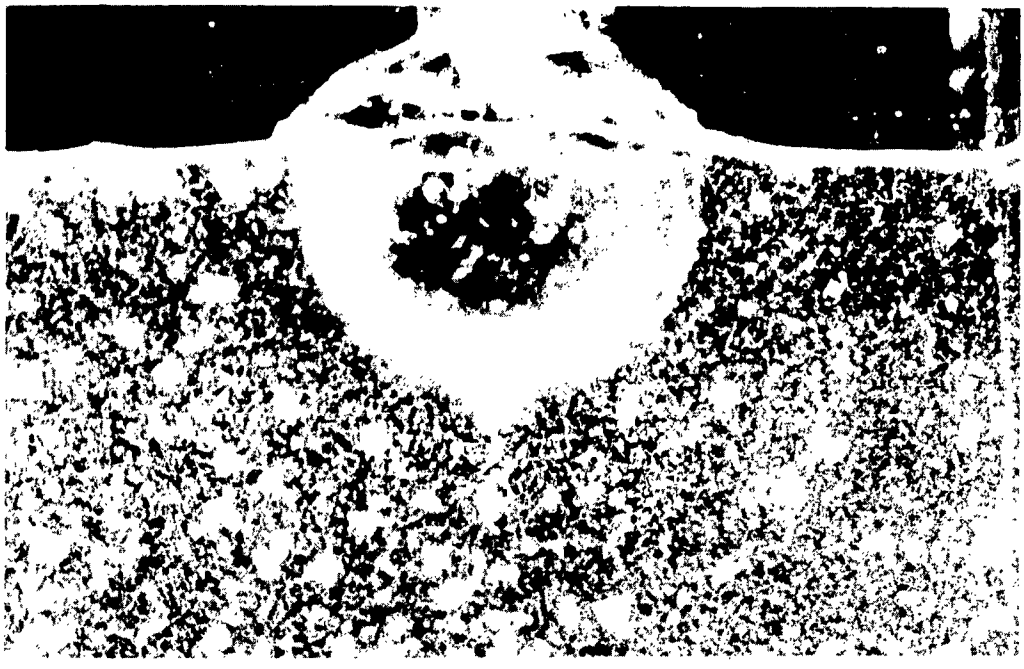

Figure 8. Cavity at maximum size; downward-moving jet just starting (64 frames/sec)

Figure 9. Cavity at maximum size; downward-moving jet well developed (64 frames/sec)

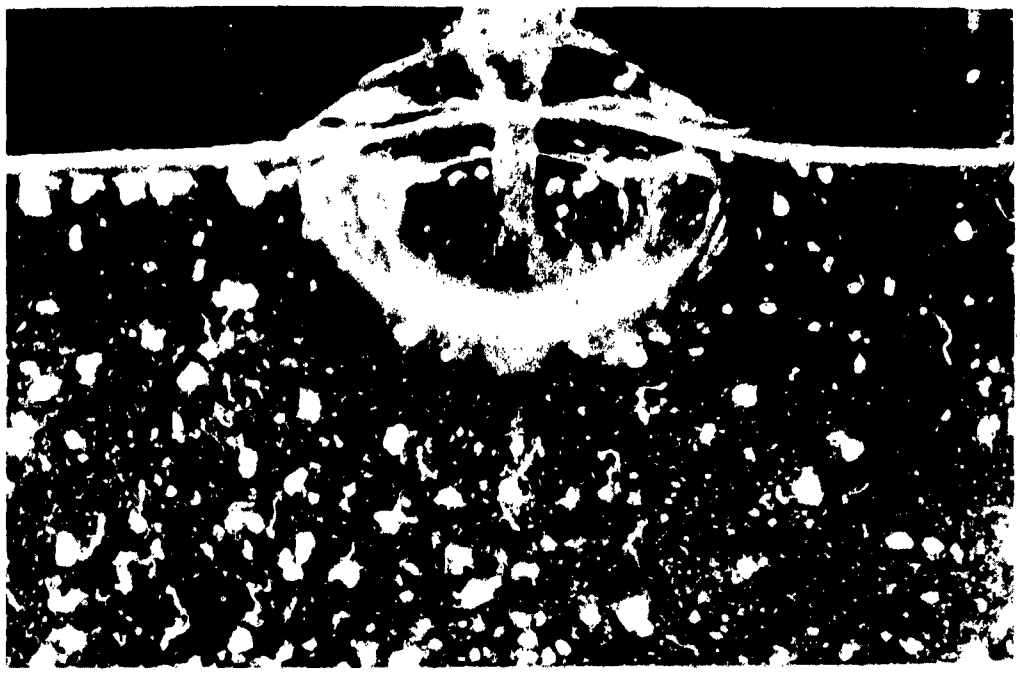

Figure 10. Cavity begins to shallow; upward-moving jet ready to emerge from cavity floor (64 frames/sec)

Figure 11. Cavity shallows further; downward- and upward-moving jets merge (8 frames/sec)

of gas or vapor contained within it. The crater produced in a liquid by impact of a liquid drop may be regarded as a half-bubble at a gas-liquid interface. When it increases in size, shear stresses are set up in the liquid in the immediate vicinity of the cavity wall. Because the liquid has essentially no strength in shear, and because the proximity of the gas phase provides an avenue of escape, the target liquid flows around the expanding cavity to form a cylindrical wave that moves up into the gas phase.

Figure 12 summarizes the flow behavior of the drop and target liquids (in idealized diagrammatic cross-sectional views) during the sequence of splash configurations produced by the impact of a liquid drop against a body of liquid. The liquid of the drop that impinged is indicated by stippling. The contour of the drop flow is obscured in the motion pictures of the impacts; the most probable contour of it is indicated with dotted lines in the cross-sectional diagrams.

Sketch A shows the impact phase of the phenomenon in which the impinging drop punches a sheer-walled cylindrical hole with flat bottom in the target liquid. The liquid of the drop that impinged flows out radially over the bottom of this disk-shaped cavity.

Sketch B shows a later stage in which the cavity has assumed hemispherical shape. A cylindrical wave has risen around it; the cylindrical wave is formed of target liquid that has flowed around the cavity. Both the cavity and the cylindrical wave are undergoing steady growth; streamlines in the target liquid are indicated with dashed lines and the direction of flow with arrow heads. The liquid of the drop that impinged has flowed out radially over the lower half of the cavity floor.

Sketch C shows a stage in which the cavity is approaching maximum size. The crest of the cylindrical wave is constricting under the force of surface tension. Streamlines in the target liquid and the direction of motion in it are indicated in the same way as in Sketch B.

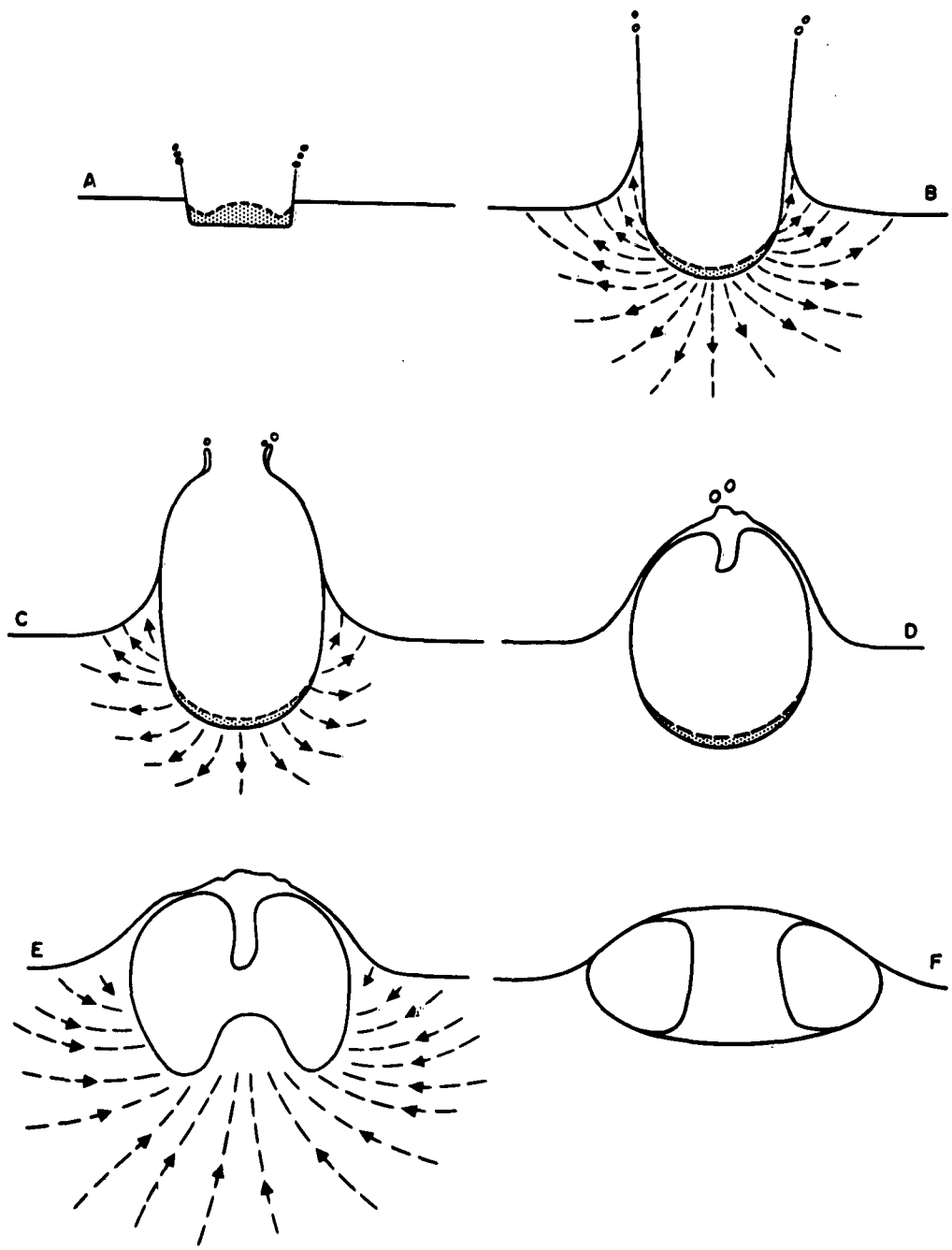

Figure 12. Cross sections of the flow stages of a liquid drop impact

Sketch D shows the cavity shortly after it has reached maximum size. The cylindrical wave has closed to form a bubble over the cavity and the downward-moving jet of liquid has been produced at the point of closure. There is no motion in the target liquid around the cavity.

Sketch E shows the dynamic recoil of the target liquid. The motion of the liquid is now in the reverse direction of what it was in Sketches B and C and an upward-moving jet has begun to rise in the center of the cavity floor. In the case of low-velocity impacts, for which the bubble closure shown in Sketch D never occurs, the upward-moving jet formed by the recoil of the target liquid simply rises up through the center of the cavity and through the center of the cylindrical wave carrying the liquid of the drop that impinged at its apex. In the case of high-velocity impacts, for which the cylindrical wave closes to form a bubble over the cavity, as shown in Sketch D, the upward-moving jet formed by the recoil of the target liquid merges with the downward-moving jet and the structure shown in Sketch F results.

The location of the liquid belonging to the drop is not indicated with stippling in Sketches E and F because the high concentration of color in the drop liquid made it impossible to obtain this information from the films that were made, and there was no objective evidence from which it could be deduced.

At long times after the impact has occurred, the bulk of the liquid of the drop eventually coalesces into a globule again, but quite a bit of it has been lost by diffusion into the target liquid in red cloud-like masses.

4. Equation for Maximum Cavity Depth

Figure 13A is a photograph of the flow configuration (cavity and cylindrical wave) formed in water as a result of the impact of a waterdrop. The glass ruler at the extreme right of the picture is graduated in millimeters.

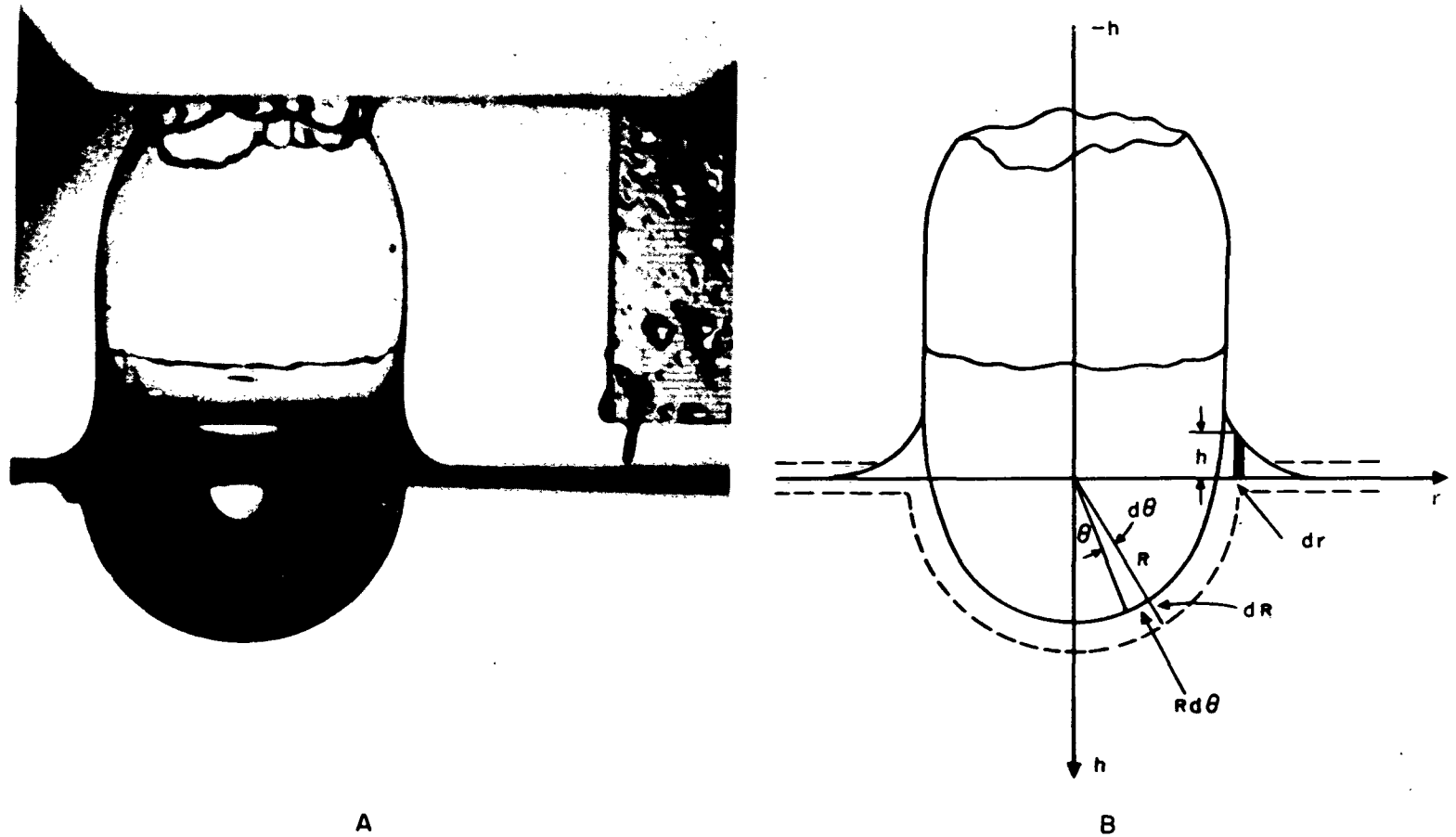

Figure 13. Cavity and cylindrical wave at time of maximum depth

A. Enlargement from high-speed moving picture. Ruler graduated in mm.
B. Tracing of A with cavity corrected for magnifying effect of water

Figure 13B is a tracing of the cavity and wave shown in Figure 13A; the depth of the cavity is corrected for the magnifying effect of the water.

The photograph of the cavity and cylindrical wave shown in Figure 13A was taken at the time of maximum cavity depth. At the time that the cavity reaches maximum depth all motion in the target liquid in the vicinity of the cavity wall has stopped and the energy given to the target liquid by the impinging drop is almost wholly transformed into potential energy. At all other times this energy is partly potential and partly kinetic. To derive an equation that will give the depth of the cavity it is necessary to obtain analytical expressions for the energy in the various forms in which it exists.

4.1 Potential Energy Due to Gravity

The gravity potential energy, U, of the cylindrical wave is the work required to lift the liquid contents of the cavity to the original undisturbed surface of the liquid and the work required to lift the cylindrical wave swell above this surface. The energy U is given by [8]

$$U = (g\,\rho/2) \int h^2 \cdot 2\,\pi\, r\, dr = \pi\, g\, \rho \int h^2\, r\, dr \qquad (1)$$

where g is the acceleration of gravity, ρ is the density of the target liquid, h is the distance from the original liquid level to the free liquid surface after impact, and r is the distance along the r-axis. See Figure 13B. To evaluate this energy it is necessary to find analytical expressions for h.

For hemispherical craters, which are observed experimentally when the drop liquid is the same as the target liquid, the curve of the cavity wall is a quadrant of a circle with center at the origin given by

$$r^2 + h^2 = R^2$$

so that

$$h^2 = R^2 - r^2 \qquad (2)$$

Substituting eq (2) into eq (1), the gravity potential energy of the cavity, U_1, is given by

$$U_1 = \pi g \rho \int_0^R (R^2 - r^2)\, r\, dr$$

$$= \pi g \rho R^4/4 = 0.2500\, \pi g \rho R^4 \qquad (3)$$

The height of the cylindrical wave must be determined from the continuity condition that the volume of the wave is equal to the volume of the cavity and that the height of the wave is zero at $r = \infty$. The volume of the wave is given by

$$2\pi \int_R^\infty h\, r\, dr$$

and since, for hemispherical craters, the volume of the cavity is $2\pi R^3/3$.

$$2\pi \int_R^\infty h\, r\, dr = 2\pi R^3/3.$$

This equality is satisfied by the expression

$$h = -R^4/3r^3 . \qquad (4)$$

This solution is not unique. However, eq (4) yields values of h that are in reasonable agreement with the observed height of the cylindrical wave in the range $r = R$ to $r = 2R$. Furthermore, eq (4) yields the result $h = 0$ when $r = \infty$. On the basis of these criteria eq (4) may be taken to be a good approximation of the height of the cylindrical wave.

Substituting eq (4) into eq (1), the gravity potential energy of the wave above the surface, U_2, is given by

$$U_2 = \pi g \rho \int_R^\infty (R^8/9\, r^6)\, r\, dr$$

$$= (\pi g \rho R^8/9) \int_R^\infty r^{-5}\, dr$$

$$= \pi g \rho R^4/36 = 0.02778\, \pi g \rho R^4. \qquad (5)$$

The crest of the cylindrical wave, which extends around the periphery of the cavity is discussed in connection with the energy due to surface tension (see section 4.2). The mass of liquid in the bubble-crest of the wave, and consequently, its potential energy due to gravity, is very small; for purposes of deriving the cavity depth equation, it has been neglected.

4.2 Potential Energy of Generated Surface

The formation of the cavity and cylindrical wave is accompanied by the generation of new surface. The energy required to form this surface is potential; it represents an important investment of transformed energy. To evaluate it, it is necessary to determine the amount of new surface that is generated.

The outside curved surface of the cylindrical wave can be found by revolving eq (4) about the h-axis (see Figure 13B). The generated surface, S, is given by

$$S = 2\pi \int_0^{R/3} r\, [1 + (dr/dh)^2]^{1/2}\, dh$$

where the upper limit of integration is the wave height, h, when r = R. To obtain the net generated surface, S_1, it is necessary to subtract the original

planar surface of the liquid which existed before the impact occurred. Then

$$S_1 = 2\pi \int_0^{R/3} r\,[1 + (dr/dh)^2]^{1/2}\,dh - 2\pi \int_R^{\infty} r\,dr$$

From eq (4),

$$dh = (R^4/r^4)\,dr$$

and

$$dr/dh = r^4/R^4.$$

Substituting these expressions and changing the limits of integration of the first term to correspond,

$$S_1 = 2\pi \left[\int_R^{\infty} (R^8 + r^8)^{1/2}\,(dr/r^3) - \int_R^{\infty} r\,dr \right]$$

$$= 2\pi \int_R^{\infty} [(R^8 + r^8)^{1/2} - r^4]\,dr/r^3$$

The integral is of a type that cannot be solved in closed form [9]. It can be solved graphically. Values of the integrand for various values of r are listed in Table 1. The area under the curve was found to be $0.0692\ R^2$ so that

$$S_1 = 2\pi\,(0.0692\ R^2) = 0.1384\,\pi\,R^2. \tag{6}$$

The area of the cavity in the target liquid is $2\pi R^2$. The net generated area in the cavity wall, S_2, is the cavity area minus the area of the original planar surface of the liquid before the impact occurred, which is πR^2. Consequently,

$$S_2 = 2\pi R^2 - \pi R^2 = \pi R^2 \tag{7}$$

The area of the vertical wall of the cylindrical wave at the periphery of the cavity, S_3, is the product of the cavity perimeter and the vertical wave height, h, at the distance r = R,

$$S_3 = 2 \pi R (R/3) = 2 \pi R^2/3 \tag{8}$$

Although the gravity potential energy of the bubble-crest of the cylindrical wave is negligible (see section 4.1), its surface energy is important.

TABLE 1

Values of the Integrand by Means of Which Surface Area S_1 was Determined

r	$[(R^8 + r^8)^{1/2} - r^4]/r^3$
1 R	0.4142 R
5 R/4	0.1008 R
4 R/3	0.0652 R
3 R/2	0.0290 R
2 R	0.0039 R
3 R	0.0002 R
4 R	0.0000_3R

The top of the wave where its nearly vertical wall that rises from the rim of the cavity meets its upper surface is sharply convex and has a vanishingly small radius of curvature. The pressure due to surface tension, which results

from this acute convexity [10], causes the bubble-thin cylinder of liquid to rise out of the top of the cylindrical wave. On the other hand, the concave shape of the lower part of the cylindrical wave produces a negative pressure or suction [10]. The bubble-thin cylinder of liquid will rise until checked by the combined action of the force of gravity and the suction due to the concave shape of the lower part of the cylindrical wave. The effect of gravity is very small; the major check is the negative pressure.

An expression that will give the height to which the bubble-thin crest of the cylindrical wave will rise has not as yet been formulated. However, for impacts of waterdrops against water, it appears from measurement data on the cavity and bubble crest that the height of the bubble crest is about equal to twice the depth of the cavity for impacts in which the kinetic energy of the impinging drop is in excess of about 50,000 ergs. Using this empirical relation and remembering that the bubble crest has two sides, the surface area of the bubble crest of the cylindrical wave, S_4, produced in impacts of waterdrops with water is

$$S_4 \cong 2\,[2\,\pi\,R\,(2\,R)] \cong 8\,\pi\,R^2. \tag{9}$$

The net generated surface of the cavity and cylindrical wave is S, and

$$S = S_1 + S_2 + S_3 + S_4.$$

From eqs (6), (7), (8), and (9).

$$S \cong 9.8051\,\pi\,R^2$$

and the potential energy due to generated surface, U_3, is

$$U_3 = 9.8051\,\pi\,R^2\,\gamma \tag{10}$$

where γ is the surface tension of the liquid.

4.3 Other Energy Sinks

Sound energy is radiated into a liquid as a result of the impact of a liquid drop. Franz [11] has found that the total sound energy radiated into water by impact of a waterdrop is approximately equal to 2 T' M^3 where T' is the kinetic energy of the impinging drop and M is the Mach Number of the drop based on the velocity of impact. The velocity acquired by a waterdrop falling freely through a distance of nearly 65 feet in a tube evacuated to the vapor pressure of water is roughly 55 ft/sec. Taking the speed of sound in the target water to be 5,000 ft/sec, M = 0.011 and M^3 = 0.0000013. It is apparent that the fraction of the kinetic energy of the drop that is converted to sound energy is very small and can be neglected without loss.

Dissipation of energy does occur. However, for liquids of low viscosity, such as water, the dissipated energy is small and may be neglected.

4.4 Equation for Maximum Cavity Depth

In order to obtain an equation for maximum cavity depth, some assumption must be made with regard to partition of the energy of the impinging drop. Let it be assumed arbitrarily that half of this energy is given to the target liquid and the other half is retained by the drop. This assumption is justified in some measure by the observation that the experimentally observed cavity wall velocity is about equal to half the impingement velocity for short times after the impact and decreases more or less regularly, thereafter. The shape of the experimental cavity-wall-versus-time curve resembles a rectangular hyperbola.

With use of this assumption, at the time of maximum cavity depth all of the potential energy that has been accounted for must equal half of the energy of the impinging drop, that is,

$$U_1 + U_2 + U_3 = \pi d^3 \delta V^2/24$$

where δ is the density of the drop liquid. Substituting the expressions for the potential energy terms from eqs (3), (5), and (10), and using R_m to denote the maximum radius of the cavity in the target liquid,

$$0.2778\ \pi\ g\ \rho\ R_m^4 + 9.8051\ \pi\ R_m^2\ \gamma = \pi\ d^3\ \delta\ V^2/24$$

If this expression is divided by $0.2778\ \pi\ g\ \rho$,

$$R_m^4 + 35.298\ \gamma\ R_m^2/g\ \rho = d^3\ \delta\ V^2/6.6667\ g\ \rho$$

By completing the square, the quartic equation in R_m can be transformed to a quadratic in R_m^2.

$$(R_m^2 + 17.649\ \gamma/g\ \rho)^2 = d^3\ \delta\ V^2/6.6667\ g\ \rho + 311.49\ \gamma^2/g^2\ \rho^2$$

from which

$$R_m = [(d^3\ \delta\ V^2/6.6667\ g\ \rho + 311.49\ \gamma^2/g^2\ \rho^2)^{1/2} - 17.649\ \gamma/g\ \rho]^{1/2} \qquad (11)$$

Values of maximum cavity depth computed with use of eq (11) for impacts of waterdrops against water are compared with experimental values of maximum cavity depth for impacts of this kind in section 6.

In using eq (11), its limitations should be remembered. One of these limitations is that the the empirical approximation used in eq (9) to make it possible to obtain eq (10) for the potential energy of surface was based only on observations of impacts of waterdrops against water and may not be true in general. Another limitation is that eqs (3) and (5) for the potential energy due to gravity were obtained for the case that the crater formed in the target liquid is hemispherical. Hemispherical craters are formed when the drop and

target are of the same liquid. Consequently, the density ratio δ/ρ in the first term on the right-hand side of eq (11) is unity for the condition under which this equation applies.

5. Craters That Are Not Hemispherical

If the density of the drop liquid is greater than that of the target liquid, the depth of the crater that is formed is greater than its radius; for this case the cross section of the crater resembles half a prolate spheroid. The craters that Rupe [12] produced in kerosene by impact of a waterdrop are of this type. To obtain a crater-depth equation for impacts of this kind, eq (2) would have to be replaced by

$$(h^2/R^2) + (r^2/b^2) = 1$$

where R is the depth of the cavity and b is the radius of the cavity at the surface. This would lead to

$$U_1 = \pi g \rho (b^2 R^2)/4$$

in place of eq (3). On comparing this expression for U_1 with that given by eq (3), it appears that the cavity radius b is some function of R and the density ratio ρ/δ. Measurement of the depth and radius of a crater formed in kerosene by impact of a waterdrop [12] produced the empirical result that $(b/R) = 0.86$. The density of kerosene is 0.82 and the density of water at 20° C is 0.998. Using these data, $(\rho_k/\delta_w) = 0.82$ and $(\rho_k/\delta_w)^{1/2} = 0.90$. Consequently, from the meager data available, $b = (\rho/\delta)R$ or $b = (\rho/\delta)^{1/2}R$. More experimental data are needed to establish the relationship.

Similarly, for the case that $\delta > \rho$, the volume of half a prolate spheroid, $2 \pi R b^2/3$, would have to be used in obtaining U_2, the potential energy of the cylindrical wave above the surface of the target liquid.

When $\delta < \rho$, then $R < b$ and the cavity should resemble half an oblate spheroid. For this case the volume of half an oblate spheroid, $2 \pi R^2 b/3$, would have to be used in obtaining U_2, the potential energy of the cylindrical wave above the surface of the target liquid.

From eq (11) it can be seen that R_m varies directly as $V^{1/2}$. This law of variation of the depth of true liquid craters with impact velocity and the form factor involving the density ratio, which was just discussed, are of interest in considering fluid-type hypervelocity craters. They will be referred to in Part III of this report in which crater depth for the liquefied-projectile liquefied-target type of cratering will be considered.

6. Test of the Cavity Depth Equations

In order to test the equation for maximum cavity depth, reliable experimental data on collisions of waterdrops with water are essential. Because quantitative data collected under carefully controlled conditions were not available, an apparatus was designed and constructed to provide gravity acceleration of drops under reduced pressure for the purpose of carrying out an exhaustive quantitative study of the impact of liquid drops against liquids.

6.1 Description of the Apparatus

The liquid drop accelerator constructed to obtain the required data consists of a vacuum-tight pipe mounted vertically over a sealed tank. The velocity acquired by a drop during fall through any given distance is greater in evacuated space than in air because drag resistance is reduced. The size of the drop can also be made larger in an evacuated space than in air because the tendency for breakup due to air currents encountered during fall through air is reduced. The lowest feasible pressure for the simple system in which both the drop and the target are of the same liquid is the room-temperature vapor pressure of the liquid being used.

The pipe and the tank are both of 5052 aluminum alloy to minimize corrosion and corrosion-induced changes in the properties of the liquid under study. Welding was accomplished with 5154 aluminum rod which is also corrosion resistant. The pipe is of seamless circular tubing with 0.64-cm (0.25-in.) wall thickness, an inside diameter of 15.2-cm (6 in.) and a total length of 20 m (66 ft). It consists of four flanged sections.

Openings in the pipe at various heights above the tank make it possible to study liquid drop impaction at four different impingement velocities. Drop-admittance ports are located between the four pipe sections and at the top of the pipe. The drop-admittance ports are 45.7-cm (18 in.) -long sections of pipe that have a short side arm welded in. The open end of the side arm is flanged, and when not in use, each port is closed vacuum tight with a flat circular cover that bears against an O-ring.

At the level of the side arm in the drop-admittance port that is being used, the lower section of the pipe is sealed off with a removable circular plate and ring that are supported by a fixed ring welded into the pipe. Vacuum tightness is insured with O-ring seals. In the center of the removable plate there is a tapered hole into which a 19/38 ground glass joint fitted with an O-ring may be inserted. The ground glass joint supports a dripper for admitting drops of a given size into the evacuated system.

The dripper consists of a pipet nozzle, two liquid reservoirs, and two stopcocks. The inner reservoir, which is located between the stopcocks, is at first empty and the stopcock that separates this reservoir from the evacuated pipe is left open. The outer liquid reservoir is separated from the inner reservoir by the stopcock furthest from the evacuated system; this reservoir is open to atmospheric pressure and is full of the liquid to be used. When a drop is to be released, the inner stopcock is closed and the liquid is admitted into the inner reservoir at the pressure that prevails within the system. Drops are admitted into the system from the inner reservoir.

The target-liquid tank is a 35.6-cm (14-in.) -diameter cylinder 55.9-cm (22 in.) high that was rolled from 1.27-cm (0.50-in.) sheet and welded. Two 30.5-cm (12-in.) side arms, which were also rolled and seamed, are welded into it. The main criterion used in choosing the diameter of the tank was that it should be large enough to minimize the effect of the container walls on the cavities formed in the target liquid by the impacts. On the basis of available information, it appeared that a diameter of 25.4 to 30.5 cm (10 to 12 in.) would be adequate for this purpose. Excessive size was avoided both to reduce problems of procurement or fabrication and to minimize the volume of target liquid that would be required for the experiment. The second consideration will be important when liquids other than water are investigated.

The open ends of the side arms in the tank terminate in 1.9-cm (0.75-in.) flanges. They are closed vacuum tight with 2.54-cm (1-in.) -thick covers that contain glass windows through which the liquid drop impacts are photographed. The windows, of No. 7913 optical grade Vycor glass, were furnished with a commercial polish. They were given an additional finish to render them sufficiently flat, symmetrical, and parallel to insure minimum distortion in the pictures. Pictures taken through the windows with a glass ruler suspended in the vertical and in the horizontal position at the center of the tank indicated that there was no measurable distortion. A picture taken with the glass ruler hanging in the vertical position but with the lower half of the ruler immersed in water indicated that cavity depth measurements would have to be multiplied by a reduction factor of 0.8536 to correct for the magnifying effect of the water.

The end of the pipe is connected to the target-liquid tank through a 15.2-cm (6-in.) aluminum ball valve equipped with natural rubber seats and seals to insure long service life in an atmosphere saturated with water vapor. With the ball valve closed, the pipe can be evacuated separately without concomitant evaporation of the target liquid and the consequent need to trap out large quantities of vapor. Evacuation is accomplished with use of an air-cooled simplex-type vacuum pump having a free air displacement of 36.8 liter/min (13 cu ft/min).

6.2 Experimental Determination of Impingement Velocity

The liquid drop impacts were photographed with use of a microsecond stroboscope that was synchronized with a moving strip of film in a high-speed camera from which the rotating prism had been removed.

The velocity at which the drop strikes the surface of the target liquid is determined from the distance traversed by the drop between the last

two consecutive frames before actual impact occurs, and from the time elapsed per frame. The distance that the drop travels is determined with reference to the glass ruler, graduated in mm, that is suspended just above the surface of the target liquid at the center of the tank (see Figure 13A). The time elapsed per frame is found from the frame height and the distance between timer marks which are formed along the edge of the film.

It was found that the drops do not detach from the dripper in an absolutely uniform way. As a result, they do not consistently strike the target liquid at the center of the tank, where the glass ruler is located, but impinge at random over an approximately 10-cm (4-in.) -diameter circle about the center of the tank. The dispersion in the drop trajectories affects the calculated impingement velocity because the distance traveled by the drop between two consecutive frames, as seen by the camera, is affected by this random change in the object distance. The measured diameter of the drop and the measured depth of the cavity that forms in the target liquid as a result of the impact are also affected. The problem can be solved by statistics. If a sufficient number of impacts is photographed, the drop having a velocity corresponding to the average velocity of the group should have struck the water surface at the center of the target liquid tank where the glass ruler is suspended. The drop whose velocity is the same as the average velocity should, therefore, be free of error caused by dispersion in the drop trajectories; measurements of the drop diameter and cavity depth made with reference to the glass ruler suspended at the center of the tank should be correct.

The statistical solution of the problem was tried first. However, after more than 230 impacts of waterdrops against water had been photographed, for four different fall heights and for three different pressures in the drop accelerator apparatus, it became apparent that it was not feasible to operate the microsecond stroboscope for the large number of impacts that would be

required in order to establish a reliable average velocity for each fall height for each of the various conditions (drop size, viscosity and surface tension of liquid used, restriction of tank dimensions, etc.) that had been planned for the complete experiment. An additional optical glass window was, therefore, installed in the bottom of the target liquid tank so that the point at which each drop impinged could be determined with use of a second camera located below the tank. Knowing the point of impingement, a correction factor can be applied to measurements made on the film. The correction factor is a magnifying or reducing factor depending on whether the drop struck on the light-source or on the camera side of tank center. The work of photographing waterdrops striking water with use of the double camera arrangement has just begun.

Data presented in this report are based on impacts that were photographed with one camera only. The average impingement velocities of waterdrops that fell four different distances through the drop accelerator tube for three different pressures maintained within the tube are listed in Table 2; the number of impacts on which each average is based is also given. In two cases the average is based on so few data points as to be questionable. An attempt has been made to improve the certainty with which the impact velocity can be known from the data at hand by reference to other information.

Photographs of the freely falling drops, which were taken just before impact with the target water occurred, showed that the drops were flattened in every case. They were very slightly flattened even when the pressure in the accelerator tube was as low as the vapor pressure of water. Although the horizontal and vertical diameters of the drops, as seen by the camera, are affected by the random change in object distance caused by the dispersion in the drop trajectories, the ratio of these diameters should not be affected.

The horizontal and vertical diameters of the drops were measured and the flatness ratio (horizontal/vertical diameter) was determined. The average flatness ratio for each height of fall and for each pressure maintained in the drop accelerator tube is listed in Table 2 and plotted against the ambient pressure in Figure 14. In Figure 14 the curves for the three fall heights intersect in a point at a flatness ratio of 1.372 and a pressure of about 975 mm mercury. This is the limit flatness ratio that the drops should have when they reach constant free fall velocity. It can be seen that all of the drops that were photographed were still in process of acceleration.

TABLE 2

Average Velocity and Flatness Ratio of Falling Waterdrops

Pressure in the Tube mm	Fall Height cm	Number of Impacts	Average Values of Velocity cm/sec	Average Values of Flatness Ratio
21.5 - 26	1935	19	1717	1.041
24 - 28	1326	10	(1481?)	1.040
24 - 27	930	19	1193	1.031
25 - 26	533	16	921	1.034
178	1935	17	1421	1.227
175 - 178	1326	20	1274	1.174
175 - 179	930	17	1096	1.110
175 - 176.5	533	16	862	1.048
atm	1935	9	(781?)	1.347
atm	1326	17	835	1.336
atm	930	14	795	1.312
atm	533	14	744	1.206

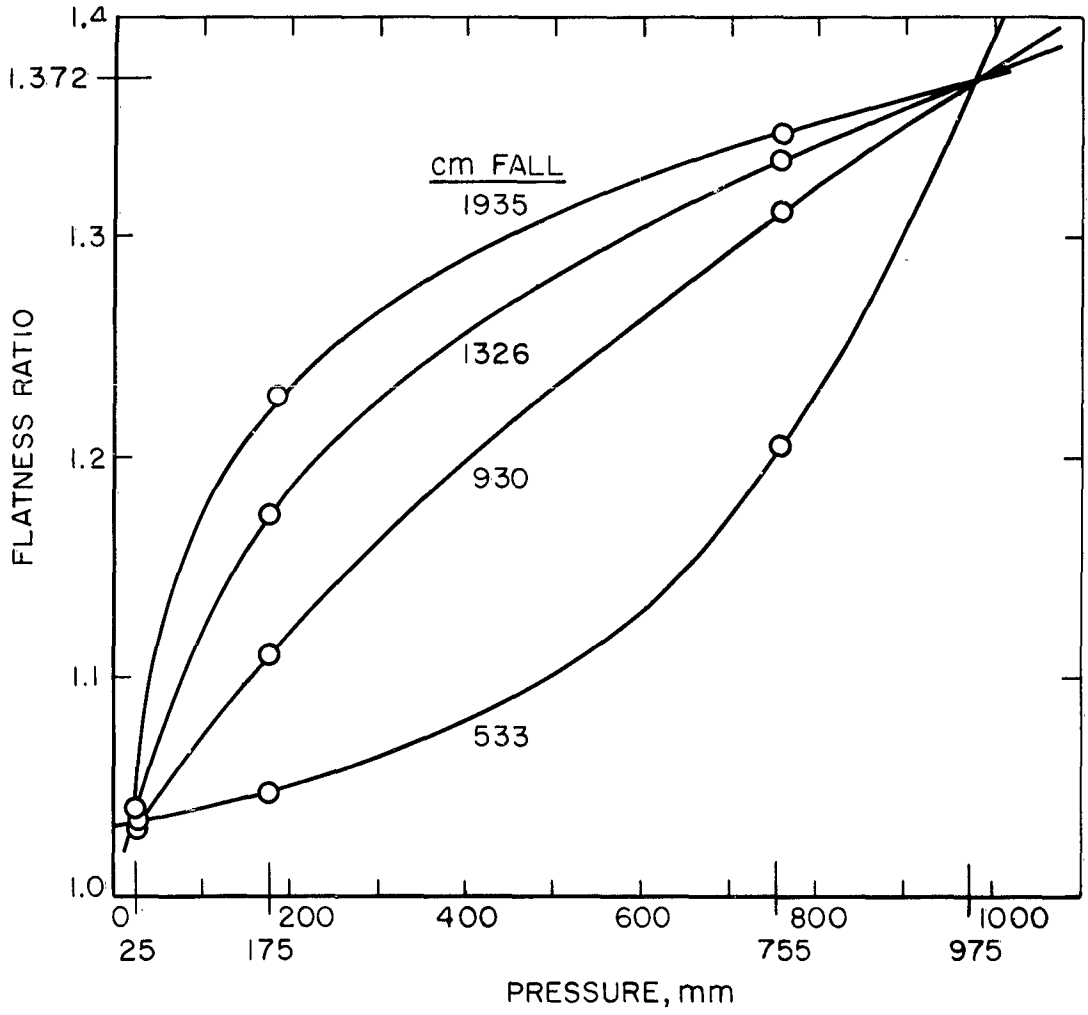

FIGURE 14. FLATNESS RATIO (HORIZONTAL/VERTICAL DIAMETER) OF FALLING WATERDROPS AT THREE DIFFERENT PRESSURES

The averages of the observed velocities for each height of fall (see Table 2) were then plotted against the ambient pressure. See Figure 15. Best fit curves were drawn so as to provide a point of intersection at the same pressure at which the flatness-ratio curves intersect in Figure 14. The constant free fall velocity indicated by this point of intersection is seen to be 725 cm/sec. From Figure 15 the velocity for the 1326-cm fall at 25 mm mercury pressure, which was indicated as questionable in Table 2 and is supported by only ten data points, is seen to be much too high. In order to avoid confusion, the velocity for the 1935-cm fall at 755 mm mercury pressure, which was also indicated as questionable and is supported by only nine data points, is not plotted; it would fall between the two lowest curves and is obviously incorrect.

The theoretical velocity acquired by a mass falling freely in a vacuum may also be used to bolster the reliability of the experimental impact velocities. This velocity is given by $\sqrt{2\,g\,s}$ where g is the acceleration of gravity and s is the fall height. The theoretical velocities that would have been acquired in fall through each of the arbitrary fall heights used, if zero pressure had been maintained in the drop accelerator apparatus, are plotted in Curve A of Figure 16. The average observed velocities for each of the pressures for which data were collected are plotted as Curves B, C, and D in Figure 16; these curves are drawn to be consistent with the curves of Figure 15. Both points that were indicated as questionable in Table 2 are plotted in Figure 16; they are indicated with a slanting bar. It can be seen that the other average values are mutually consistent and in agreement with the theoretical curve. Velocities read from the curves of Figure 16 should be more reliable than any of the separate average velocities on which they are based.

After the data reported in Table 2 had been collected, it was discovered that the timer, which had been used in photographing all of the impacts, was

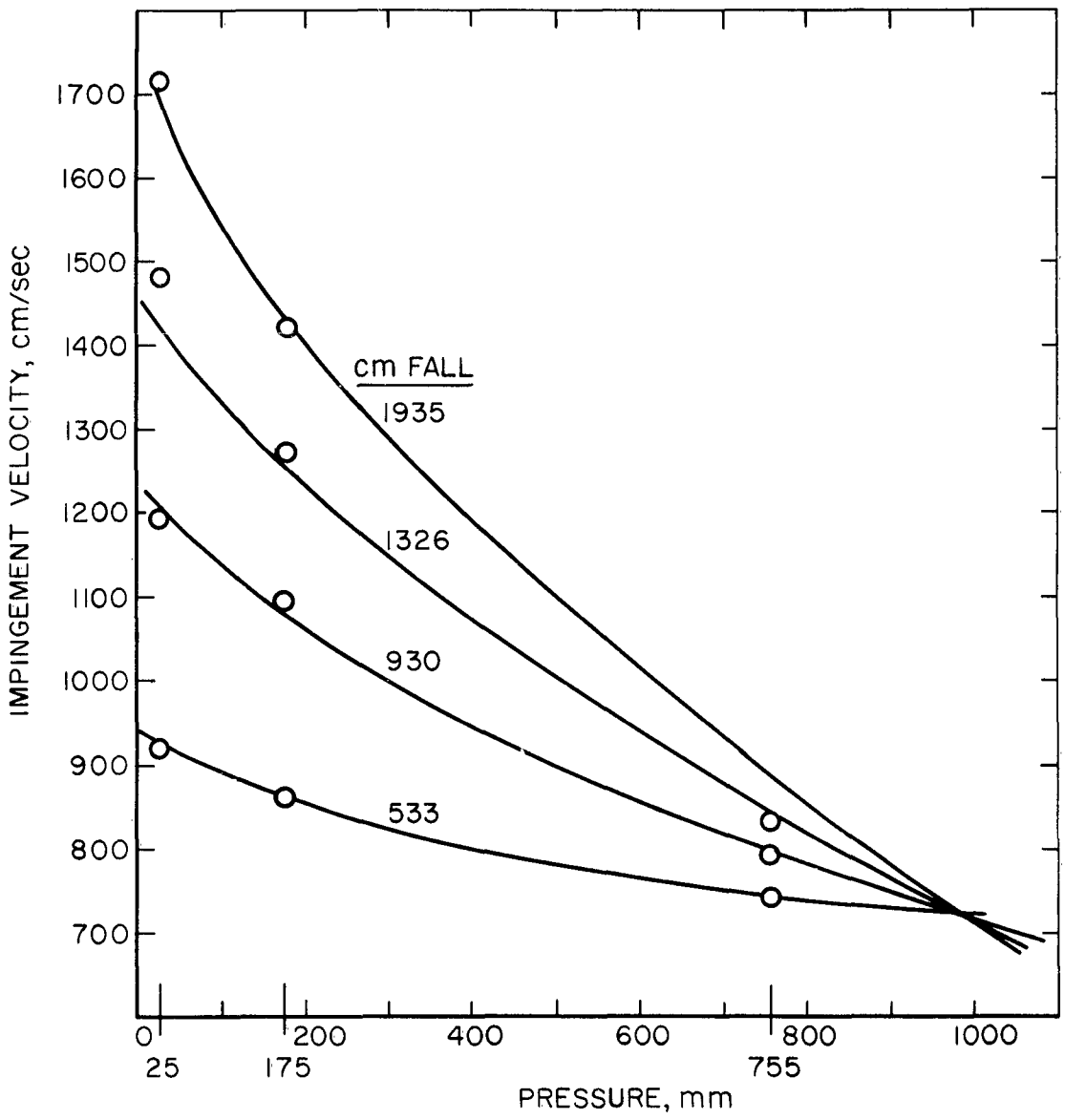

FIGURE 15. VELOCITY ACQUIRED BY WATERDROPS AT THREE DIFFERENT PRESSURES FOR FOUR DIFFERENT FALL HEIGHTS

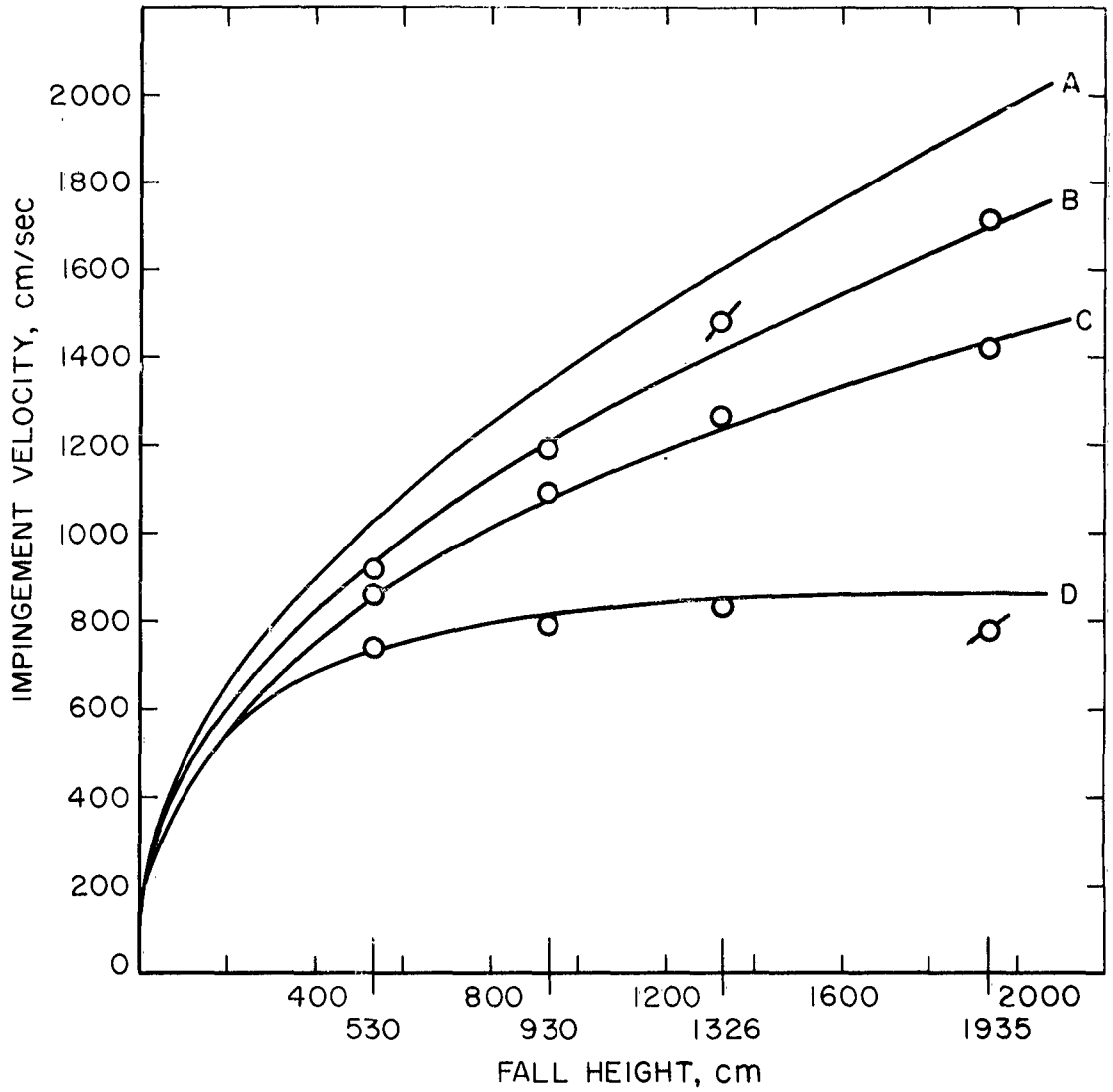

CURVE A VACUUM
CURVE B 25 mm MERCURY
CURVE C 175 mm MERCURY
CURVE D ATMOSPHERIC PRESSURE

FIGURE 16. VELOCITY ACQUIRED BY WATERDROPS DURING FALL FROM FROM FOUR HEIGHTS AT FOUR DIFFERENT PRESSURES

giving an inconsistent response, which was always less than the expected millisecond. The trouble was eventually traced to gradual failure of a vacuum tube. Because the timer was giving a low response, the recorded velocities, which were seen to be consistent among themselves, are presumably all low. The extent of the discrepancy can only be assessed qualitatively.

Laws [13] has tabulated the velocities acquired by waterdrops of different sizes on falling various distances through air at atmospheric pressure. These data were obtained in a study carried out at the Hydraulics Laboratory of the National Bureau of Standards. Interpolation of these data to the drop sizes and fall heights used for the waterdrop impacts at atmospheric pressure reported here indicates that the average velocities given in Table 2 for atmospheric pressure may be low by as much as 7 to 8 per cent. It is important to note, however, that Laws [13] states that he observed velocities fully 15 per cent higher than those observed by Lenard [14] and Schmidt [15] whose results closely confirmed each other.

An independent check is afforded by measurement data on one waterdrop impact that was photographed with the double camera arrangement and with use of the NBS 1000-cycle signal as a timer. This impact is discussed in detail in the following section. Measurement data for this impact, which occurred after the drop had fallen 1935-cm with a pressure of 35 mm mercury in the system, indicates that the impact velocity for this pressure and height of fall is 1761 cm/sec. This is about 2.5 per cent higher than the average velocity reported in Table 2 for the 1935-cm fall at a pressure of 21.5 to 26 mm mercury pressure.

6.3 Experimental Check of Eq (11) for Maximum Cavity Depth

For each combination of fall height and ambient pressure used, specific impacts were selected which had measured velocities close to the average

velocity for the group. It is thought that these selected impacts occurred near the center of the tank, where the glass ruler was suspended. To the extent that this is exactly the case, measured values of maximum cavity depth for these selected impacts should be correct.

The diameter of the equivalent spherical drop was computed for each selected impact. This is $(a^2b)^{1/3}$ where a is the measured major axis and b is the measured minor axis of the drop. Values of the maximum cavity depth, diameter of the equivalent spherical drop, and the measured velocity of each selected impact are given in Table 3.

For $g = 980.095$ at NBS, and taking $\delta = \rho = 1$ and $\gamma = 72$ for collisions of waterdrops with water, eq (11) reduces to

$$R_m = ([0.00015304562\ d^3\ V^2 + 1.68101952]^{1/2} - 1.2965)^{1/2}$$

Values of maximum cavity depth were computed from this form of eq (11) using the average velocity for the pressure-height combination given in Table 2 and the diameter of the equivalent spherical drop given in Table 3. The calculated values of maximum cavity depth are listed beside the observed values in Table 3.

Comparison of the calculated with the observed maximum depth values shows that the calculated values are high for the highest impact velocities and low for the lowest impact velocities; the same drift is evident for each pressure used in the drop accelerator tube. It is true that the average impact velocities given in Table 2, which were used to calculate the maximum depth values, are almost certainly still in error due to the dispersion in the drop trajectories. The extent of this error will only be known when more exact velocity data using the double camera arrangement for photographing the drops and using the NBS 1000-cycle signal for a timer become available. The velocity

data for the high fall heights are more subject to this error than those for the low fall heights, and, consequently, the disagreement between the observed and calculated cavity depth could be expected to be larger for the high heights of fall. But this should not produce a systematic drift in the difference between the observed and calculated depths at each pressure; a systematic drift is observed in Table 3.

TABLE 3

Calculated and Observed Cavity Depth for Specific Impacts of Waterdrops Against Water

Pressure in Tube mm	Fall Height cm	Velocity cm/sec	Drop Radius $(a^2b)^{1/3}$ cm	Observed Maximum Cavity Depth cm	Calculated Maximum Cavity Depth cm
22.0	1935	1756	0.466	2.09	2.36
24.0	1326	1483	0.485	1.87	2.24
24.5	930	1200	0.416	1.67	1.69
25.0	533	919	0.464	1.58	1.59
178.0	1935	1424	0.468	1.89	2.12
175.2	1326	1244	0.469	1.78	1.98
179.0	930	1087	0.472	1.71	1.81
175.0	533	861	0.463	1.60	1.52
atm	1935	--	--	--	--
atm	1326	838	0.495	1.50	1.59
atm	930	799	0.440	1.47	1.36
atm	533	740	0.444	1.37	1.31

It is possible that the use of the assumption that the height of the bubble crest of the cylindrical wave is about twice the depth of the cavity,

which was made in obtaining eq (9), may be responsible for the observed drift. The use of this assumption overestimates the potential energy due to generated surface for low heights of fall and underestimates it for large fall heights. If this is the source of the observed drift, it will be necessary to find the exact relation between the height of the bubble crest of the wave and the impact energy in order to eliminate it.

6.4 Experimental Time Dependence of Cavity Depth

As noted above, measurement data are available for one impact of a waterdrop against water photographed with a double camera arrangement and with use of the NBS 1000-cycle signal as a timer. This impact was photographed at the time that the color films discussed in section 2 were made. The fall height was 1935-cm, the pressure in the apparatus was 35 mm mercury, and the temperature was 20.1°C. From the pictures taken by the camera below the target-liquid tank, it was found that the impact occurred 1.74 cm on the camera side of the glass ruler.

Using the measured height of a frame and the distance between the timer marks along the edge of the film at the point where the impact occurred, it was found that the elapsed time per frame was 2.744 millisecond. The last measurable distance between the bottom of the drop and the surface of the target water, corrected for the 1.74-cm displacement of the impact, was found to be 0.4833 cm. From the distance traveled per frame and the time elapsed per frame, the impact velocity was found to be 1761 cm/sec. The vertical diameter of the drop was found to be equal to the horizontal diameter; the measured diameter, corrected for the 1.74-cm displacement of the impact, was found to be 0.4549 cm.

Measurements of the cavity depth and diameter were made at regular intervals for 200 frames after the impact occurred. The cavity depth

measurements, corrected for the 1.74-cm displacement of the impact and for the magnifying effect of the water, are listed in Table 4. It was only possible to measure the height of the cylindrical wave through the first 46 frames; in later frames the crest of the cylindrical wave was no longer visible.

The ratios, wave height/cavity depth and cavity depth/cavity diameter, are plotted against elapsed time in Figure 17. The ratio of wave height/cavity depth, for the 46 frames in which it could be determined, is seen to remain fairly constant at about 2, which is in agreement with the assumption made (see section 4.2) in obtaining the potential energy of surface. In Figure 17 it can be seen that the cavity depth/diameter ratio rises rapidly and overshoots the value of 0.5 for a hemispherical shape. It reaches a value of 0.6 in about 2 msec and then decays slowly; it has the value of 0.5 at the time that the cavity reaches maximum depth 30 msec after the impact occurred.

After the cavity reaches maximum depth, the target liquid undergoes a dynamic recoil (see Figure 12). The central jet that emerges from the bottom of the cavity can just be seen through the bubble-thin crest of the cylindrical wave 83.7 msec after the impact occurred; this is 53.7 msec after the cavity reached maximum depth. It is necessary for the jet to rise through the shallowed cavity and through the thickened lower part of the cylindrical wave before it can be seen through the extruded bubble crest of the wave.

Values of the cavity depth listed in Table 4 are plotted against the elapsed time in Figure 18.

7. Areas Recommended for Further Study

The limits within which eq (11) is applicable were set forth at the end of section 4.4 One of these limits is that it applies only to a hemispherical

TABLE 4

Cavity Depth at Various Periods of Elapsed Time

Elapsed Time msec	Cavity Depth cm	Elapsed Time msec	Cavith Depth cm
0.2744	0.22	14.82	2.12
0.5488	0.44	15.37	2.13
0.8232	0.652	15.92	2.17
1.098	0.789	16.46	2.16
1.372	0.865	17.01	2.20
1.646	0.957	17.56	2.20
1.921	1.03	18.11	2.19
2.195	1.10	18.66	2.22
2.470	1.13	19.21	2.26
2.744	1.18	19.76	2.25
3.018	1.24	20.31	2.22
3.293	1.29	20.85	2.30
3.567	1.32	21.40	2.31
3.842	1.35	21.95	2.30
4.116	1.40	22.50	2.33
4.390	1.45	23.05	2.27
4.665	1.45	23.60	2.33
4.939	1.48	24.15	2.35
5.214	1.52	24.70	2.33
5.488	1.56	25.24	2.37
5.762	1.58	25.79	2.33
6.037	1.60	26.34	2.34
6.311	1.62	26.89	2.34
--	--	27.44	2.35
6.586	1.66	27.99	2.35
7.134	1.70	28.54	2.38
7.683	1.74	29.09	2.35
8.232	1.78	29.64	2.37
8.781	1.82	--	--
9.330	1.84	30.18 t, max	2.36 R, max
9.878	1.87	31.56	2.33
10.43	1.90	32.93	2.31
10.98	1.95	34.30	2.28
11.52	1.98	35.67	2.31
12.07	1.99	37.04	2.27
12.62	2.05	38.42	2.22
13.17	2.05	39.79	2.20
13.72	2.08	41.16	2.17
14.27	2.08	--	--
		43.90	2.03
		46.65	2.00
		49.39	1.84
		52.14	1.72
		54.88	1.60

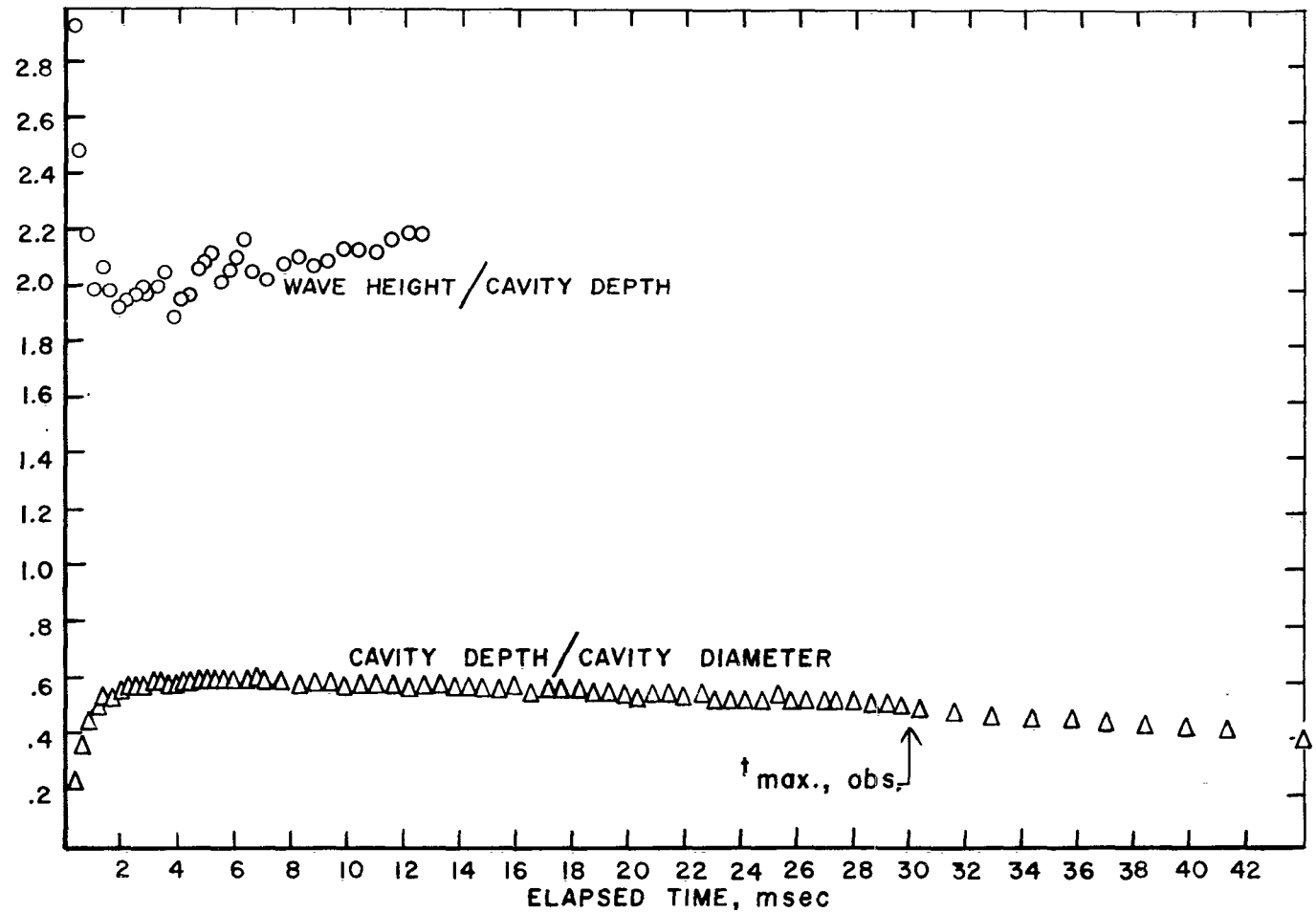

FIGURE 17 DIMENSIONLESS RATIOS INVOLVING CAVITY DEPTH

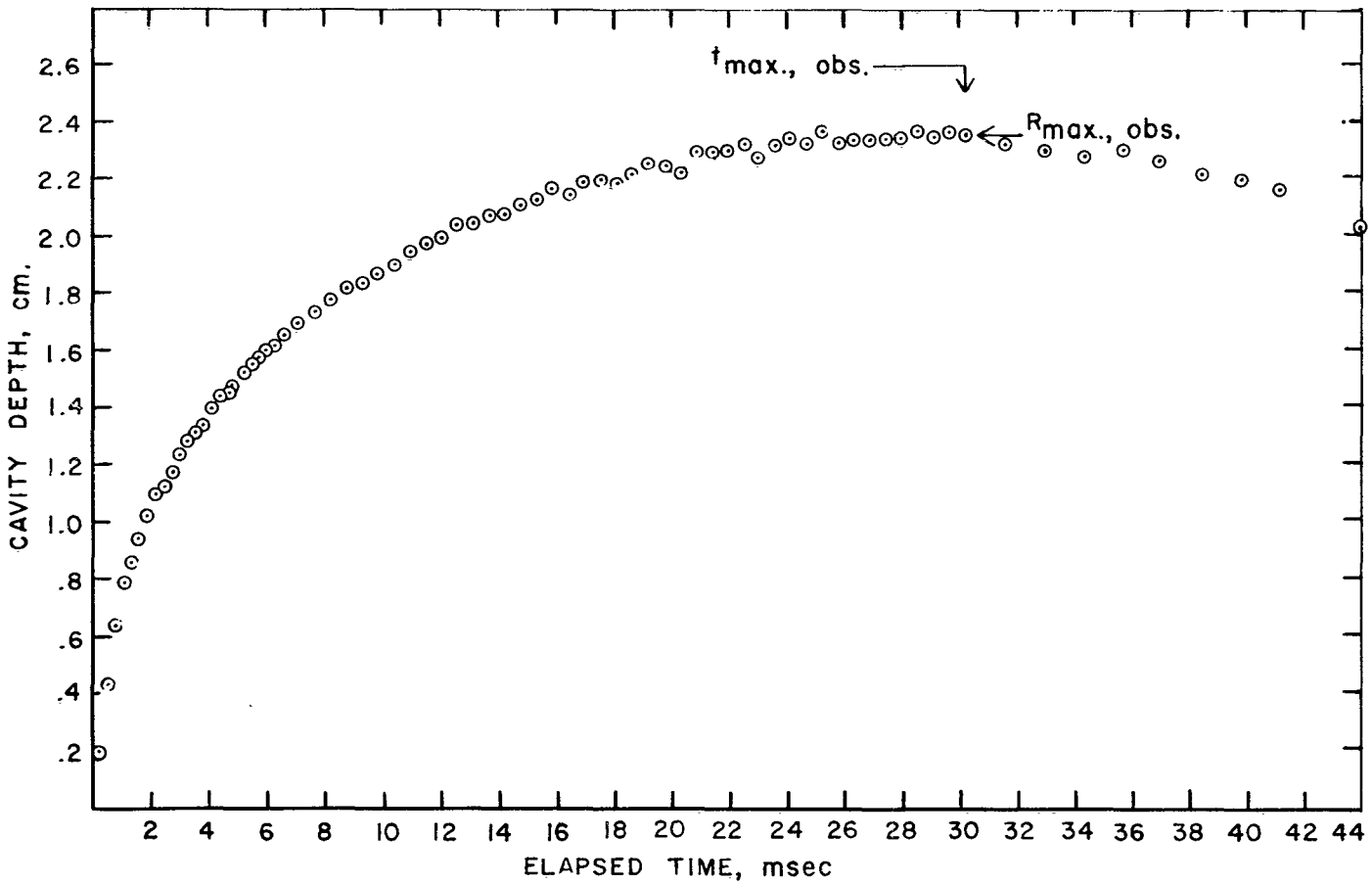

FIGURE 18. CAVITY DEPTH AT VARIOUS TIMES AFTER THE IMPACT OCCURRED

cavity. It is recommended that the flow of an impinging drop, the density of which is different from that of the target liquid, should be investigated, and that the flow of the target liquid around the resulting oblate and prolate spheroidal cavities should be studied in the same way that the flow around a hemispherical cavity has been studied in section 3. The theoretical solution for maximum cavity depth should be extended to include these cases.

Equation (11) should be tested with use of liquids of different viscosity and surface tension. The effect of the proximity of container walls on the splash phenomenon and on maximum cavity depth should also be explored. In particular, the limiting case of impingement of a liquid drop against a few drops of liquid contained in hemispherical hollows of different sizes in a glass or transparent plastic block should be studied.

From the standpoint of basic research, the time required both for closure of the bubble-crest of the cylindrical wave to form a bubble dome over the cavity in true liquid impacts, and the time required for formation of the downward-moving and upward-moving jets in these impacts should be studied quantitatively.

Another limitation of eq (11) that was cited at the end of section 4.4 is the use of an empirical relation in the development of eq (9). Recourse was had to the empirical relation because the theory behind the extrusion of bubble-thin liquid sheets from sharp-pointed liquid boundaries does not appear to have been given much study and time was not available to explore it.

The phenomenon of extrusion of bubble-thin liquid sheets from sharp-pointed liquid boundaries also occurs in the formation of vortex rings. The entire field of investigation related to the mechanics of drops and bubbles, to which this phenomenon belongs, has been neglected and is in a poorly developed state. Quite apart from its application to impacts of liquid drops against liquids, the mechanics of drops and bubbles is of major importance in the study of meteorites and of the origin of tectites as well as in more economically practical problems such as cavitation erosion and the erosion due to the impingement of liquid drops. This important area of research should be explored systematically.

List of References

1. Engel, Olive G., Symposium on Erosion and Cavitation, ASTM Special Technical Publication No. 307, 1961.

2. Öpik, E., Researches on the physical theory of meteor phenomena I, Toimetused Acta et Commentationes, Universitatis Tartuensis, XXX / A / 4 (1936) (Tartu, Estonia).

3. Engel, Olive G., NBS Technical Note 89, May 1961.

4. Worthington, A. M., On impact with a liquid surface, Proc. Roy. Soc. 34, 217 (1882).

5. Worthington, A. M., and Cole, R. S., Impact with a liquid surface, studied by the aid of instantaneous photography, Phil. Trans. Roy. Soc. 189A, 137 (1897).

6. Worthington, A. M., A Study of Splashes, (Longmans, Green, and Company, New York, 1908).

7. Worthington, A. M., On the forms assumed by drops of liquids falling vertically on a horizontal plate, Proc. Roy. Soc. 25, 261 (1877); 25, 498 (1877).

8. Lamb, Horace, Hydrodynamics, 5th Ed., Cambridge University Press, 1924. See Ch. IX, section 230.

9. Goursat, Edouard, A Course in Mathematical Analysis, Vol. I (translated by E. R. Hedrick, Ginn and Co., New York, 1904). See section 109 on integrals of binomial differentials.

10. Gibbs, J. Willard, Collected Works, (Longmans, Green, and Company, New York, 1928). See "Liquid Films" in section on Equilibrium of Heterogeneous Substances.

11. Franz, G. J., Splashes as sources of sound in liquids, Jour. Acoustical Soc. of America 31, 1080 (1959).

12. Jack H. Rupe, Critical impact velocities of water droplets as a problem in injector-spray sampling, Progress Report No. 4-80, Jet Propulsion Laboratory, California Institute of Technology, Pasadena, California, September 29, 1950.

13. Laws, J. Otis, Measurement of the fall-velocity of water-drops and raindrops, Trans. American Geophysical Union 22, 709 (1941).

14. Lenard, P., Ueber Regen, Met. Zs., v. 21, 248 (1904).

15. Schmidt, W., Eine unmittelbare Bestimmung der Fallgeschwindigkeit von Regentropfen, Sitz. Ber. Math. Naturwiss. Klasse K. Akad. Wiss., Bd 118, Abt. IIa, Wien, 1909.

Aeronautical Systems Division, Dir/Materials and Processes, Nonmetallic Materials Lab, Wright-Patterson AFB, Ohio. Rpt Nr WADD-TR-60-475, COLLISIONS OF LIQUID DROPS WITH LIQUIDS. Part II - CRATER DEPTH IN FLUID IMPACTS. Final Report, Oct. 62, 52 p., incl., illus., tables, 15 references.

Unclassified Report

Results of the use of high-speed and low-speed motion picture photography and of high-speed color photography to determine the flow configuration of both the drop and target liquids, when a liquid drop impinges against a body of liquid, are described.

A theoretical treatment of the depth of the cavity that forms in a target liquid as a result of the impact of a liquid drop is developed. Results of preliminary tests of the question are presented and discussed.

1. Motion picture photography (high and low speed)
2. Color photography (high-speed)
3. Liquids

I. AFSC Project 7342 Task 734202
II. Contract AF 33(657) 62-385
III. National Bureau of Standards, Washington, D.C.
IV. Olive G. Engel
V. Not aval fr OTS
VI. In ASTIA collection

Aeronautical Systems Division, Dir/Materials and Processes, Nonmetallic Materials Lab, Wright-Patterson AFB, Ohio. Rpt Nr WADD-TR-60-475, COLLISIONS OF LIQUID DROPS WITH LIQUIDS. Part II - CRATER DEPTH IN FLUID IMPACTS. Final Report, Oct. 62, 52 p., incl., illus., tables, 15 references.

Unclassified Report

Results of the use of high-speed and low-speed motion picture photography and of high-speed color photography to determine the flow configuration of both the drop and target liquids, when a liquid drop impinges against a body of liquid, are described.

A theoretical treatment of the depth of the cavity that forms in a target liquid as a result of the impact of a liquid drop is developed. Results of preliminary tests of the question are presented and discussed.

1. Motion picture photography (high and low speed)
2. Color photography (high-speed)
3. Liquids

I. AFSC Project 7342 Task 734202
II. Contract AF 33(657) 62-385
III. National Bureau of Standards, Washington, D.C.
IV. Olive G. Engel
V. Not aval fr OTS
VI. In ASTIA collection